AD-A138 593 UNSTEADY SEPARATED FLOWS: VORTICITY AND TURBULENCE(U) 1/1
COLORADO UNIV AT BOULDER DEPT OF AEROSPACE ENGINEERING
SCIENCES M W LUTTGES ET AL. OCT 82 AFOSR-TR-84-0120
UNCLASSIFIED F49620-83-K-0009 F/G 20/4 NL

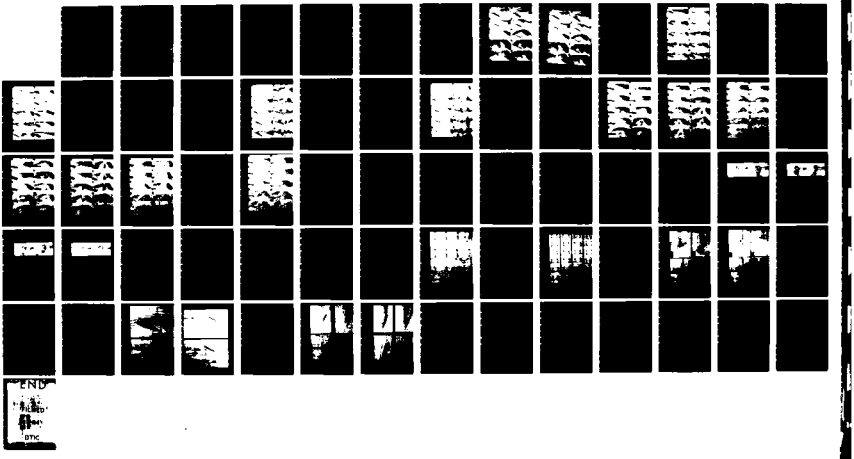

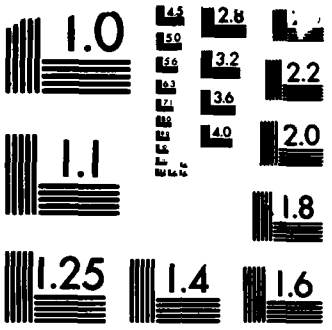

MICROCOPY RESOLUTION TEST CHART
NATIONAL BUREAU OF STANDARDS-1963-A

UNCLASSIFIED

SECURITY CLASSIFICATION OF THIS PAGE (When Data Entered)

REPORT DOCUMENTATION PAGE

READ INSTRUCTIONS BEFORE COMPLETING FORM

1. REPORT NUMBER: AFOSR-TR- 84-0120	2. GOVT ACCESSION NO.: AD-A138593
3. RECIPIENT'S CATALOG NUMBER:	
4. TITLE (and Subtitle): UNSTEADY SEPARATED FLOWS: VORTICITY AND TURBULENCE	5. TYPE OF REPORT & PERIOD COVERED: FINAL 1 Nov 80 - 31 Oct 82
	6. PERFORMING ORG. REPORT NUMBER:
7. AUTHOR(s): M W LUTTGES, C Y CHOW, D A KENNEDY, P FREYMUTH	8. CONTRACT OR GRANT NUMBER(s): AFOSR-81-0037
9. PERFORMING ORGANIZATION NAME AND ADDRESS: UNIVERSITY OF COLORADO, DEPARTMENT OF AEROSPACE ENGINEERING SCIENCES, BOULDER, CO 80309	10. PROGRAM ELEMENT, PROJECT, TASK AREA & WORK UNIT NUMBERS: 61102F, 2307/A2
11. CONTROLLING OFFICE NAME AND ADDRESS: AIR FORCE OFFICE OF SCIENTIFIC RESEARCH/NA, BOLLING AFB, DC 20332	12. REPORT DATE: October 1982
	13. NUMBER OF PAGES: 66
14. MONITORING AGENCY NAME & ADDRESS(if different from Controlling Office):	15. SECURITY CLASS. (of this report): Unclassified
	15a. DECLASSIFICATION/DOWNGRADING SCHEDULE:

16. DISTRIBUTION STATEMENT (of this Report)

Approved for Public Release; Distribution Unlimited.

17. DISTRIBUTION STATEMENT (of the abstract entered in Block 20, if different from Report)

DTIC ELECTE MAR 6 1984 A

18. SUPPLEMENTARY NOTES

Copy available to DTIC does not permit fully legible reproduction

19. KEY WORDS (Continue on reverse side if necessary and identify by block number)

FLUID MECHANICS
UNSTEADY AERODYNAMICS
UNSTEADY FLOWS
SHEAR FLOWS
OSCILLATING AIRFOILS
DYNAMIC STALL

20. ABSTRACT (Continue on reverse side if necessary and identify by block number)

Recent research progress on this multi-investigator program in unsteady separated flows is summarized. Specific projects reviewed include: (a) oscillating airfoil dynamic stall; (b) vortex entrapment and stability analysis; and (c) natural flight lift mechanisms. Research is continued under AFOSR contract F49620-83-K-0009.

DD FORM 1 JAN 73 1473 EDITION OF 1 NOV 65 IS OBSOLETE

UNCLASSIFIED

SECURITY CLASSIFICATION OF THIS PAGE (When Data Entered)

DISCLAIMER NOTICE

THIS DOCUMENT IS BEST QUALITY PRACTICABLE. THE COPY FURNISHED TO DTIC CONTAINED A SIGNIFICANT NUMBER OF PAGES WHICH DO NOT REPRODUCE LEGIBLY.

FINAL

Unsteady Separated Flows: Vorticity and Turbulence

Sponsored by: USAFOSR
Dr. Michael Francis
Project Manager

Progress Report
Nov. 1981-Oct. 1982

AFOSR contract #-
F49620-83-K-0009 and
AFOSR grant #-
AFOSR-81-0037

Co-Principal Investigators:
M. W. Luttges
C. Y. Chow
D. A. Kennedy
P. Freymuth

Summary

During the last fiscal year Professor P. Freymuth joined our research effort. His work has progressed well and is rapidly filling in a crucial gap in our integrated research project. The other portions of the project are now fully mature. Experimental work on oscillating airfoils, oscillating plates, oscillating wings and insect flight mechanisms is being brought to fruition as evidenced by the manuscripts and papers attached in the appendix of this report. Many additional papers are being finished. Perhaps most importantly, all elements of the experimental work are beginning to merge into a single coherent picture of fundamental characteristics of unsteady flow mechanisms. At this point we are beginning to consider explicit means through which our experimental models can be committed to computational extrapolations and numerical models.

The recent addition of graduate students from the Air Force Academy in our research program aids in more rapid completion of existing work and in the extension of experimental work. Close working relations with the Seiler Laboratory at the Air Force Academy are especially evident with H. Helin's work. He is initiating a comprehensive program of flow visualization using the unique experimental mechanism originated by Dr. Francis. The visualization will include a range of airfoil accelerations and pitching motions which are of great experimental importance but which cannot be readily tested

in our existing facilities. Nevertheless, the results of these experiments will be of direct significance to our existing and ongoing experimentation.

Our work in the two-dimensional consideration of unsteady separated flow is sufficiently well-developed that additional studies will focus upon specific quantifications and carefully selected dynamic conditions permitting exploitation of the observed phenomena. The new directions will emphasize the flow dynamics characteristic of three-dimensional structures produced by unsteady, separated perturbations of the flow. Our initial studies in these areas indicate that wingtip vorticity and pitching vorticity may interact in a way which reduces the undesirable drag and cataclysmic separation, respectively, of each. Even now it is clear that the interaction between these types of vorticity results in flow structures which are not a simple reflection of adding the two types of vortical flows together. To some extent this observation could have been predicted from studies focused upon the need for end-plates. Additional elaboration of these studies is planned.

Studies of insect flight mechanisms have resulted in one manuscript and another is planned. These studies reveal a wealth of wing-flow interactions which may be responsible for the lift generated by these insects. We are continuing to analyse both our videotaped records and photographs to ascertain all possible mechanisms operating in lift generation. Our model of vortical interactions with the two sets of wings appears fundamentally valid but many sophisticated modifications of this model also seem to be operating. Variations in wing geometry throughout the wingbeat cycle appear crucial. The spanwise flow of distortion and the variable camber of the wing have definite implications for the manner in which vorticity is trapped over the wing and allowed to work upon the wing. The interaction of vorticity with the wings must, of course, be considered with regard to the presence of wing tip vortices. Separated

elements of these postulated interactions can be evaluated independently in our wind-tunnel and/or zero flow experiments.

Acceleration experiments have demonstrated the evolution of vorticity around an airfoil set at a variety of angles of attack. The vortex sheets merge into progressively larger structures as acceleration continues. At sufficiently high flow velocities the flow is dominated by Karman Vortex Streets. Only now have these observations been solidified to the point that airfoil force balance measurements will be made. Of major interest in this work is the relationship between the acceleration-dependent vorticity and the vorticity visualized in experiments using the pitching airfoil. It is clear that the acceleration applied to flow impinging on an airfoil results in fluid stresses and vorticity regardless of the mechanism generating such acceleration. This common focus of our two different experiments is being examined in detail by bringing the test conditions for these experiments quite close together. As might be expected, the acceleration conditions also exhibit flow structure characteristics similar to those generated by oscillating plates in a zero flow condition. In this case, vortical interactions bounded by the plate geometry are quite contained or fixed spatially. The synthesis of these approaches will be crucial to understanding aerodynamically exploitable flows.

Theoretical studies are progressing rapidly. A number of manuscripts and publications have been generated. It is expected that the experimental work is of sufficient maturity that theoretical work will use these data for exploring novel and oscillatory lift enhancement mechanisms. The availability of experimental data which goes quite far beyond available published literature coincides with the development of theoretical methods for meaningful treatment of such data.

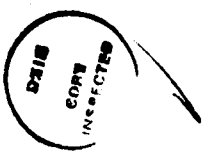

Flow Perturbations Induced by Oscillating Airfoils and Plates

Throughout the last year we have attempted to fully document the flow perturbations elicited by unsteady motions of both airfoils and plates. A wide range of dynamic parameters were investigated. Some of these data were reported recently (Robinson and Luttges, 1983) at an AIAA conference. Much of the data of this report, however, has not been reported and constitutes the bulk of manuscripts being prepared.

The flow visualizations have been corroborated (for apparent flow velocities and size) using hotwire anemometry at select points in the flow. The tests were all completed in the low-turbulence, 2'x2' test section wind tunnel at the University of Colorado, Boulder. The airfoils tested consisted of a 6" chord NACA 0015 airfoil (with and without endplates) and a 10" chord NACA 0012 airfoil. Both airfoils were 2' long and spanned the whole test section. The flat plates were 1/4" thick with leading and trailing edge geometries which were exactly the same as those of a NACA 0015 cross section at the trailing edge. The plates had 6" and 12" chord lengths, respectively. In addition, the plates could be oscillated roughly about either the 1/4, 1/2 or 3/4 chord positions. The airfoils, by a 180° turn, could be oscillated about the 1/4 (normal) or 3/4 chord (reversed) points.

With our experimental configuration, the dynamic unsteadiness variables of oscillation rate and oscillation angle can be altered from 0-12 Hz. and $\pm 0^{\circ}$-$\pm 10^{\circ}$, respectively. The Re number, with appropriate chord length, could be raised to approximately 250,000 with usable flow visualization and corresponding anemometry. The next series of flow visualizations exploit all of these variables in systematic relation to the underlying flow perturbation parameters.

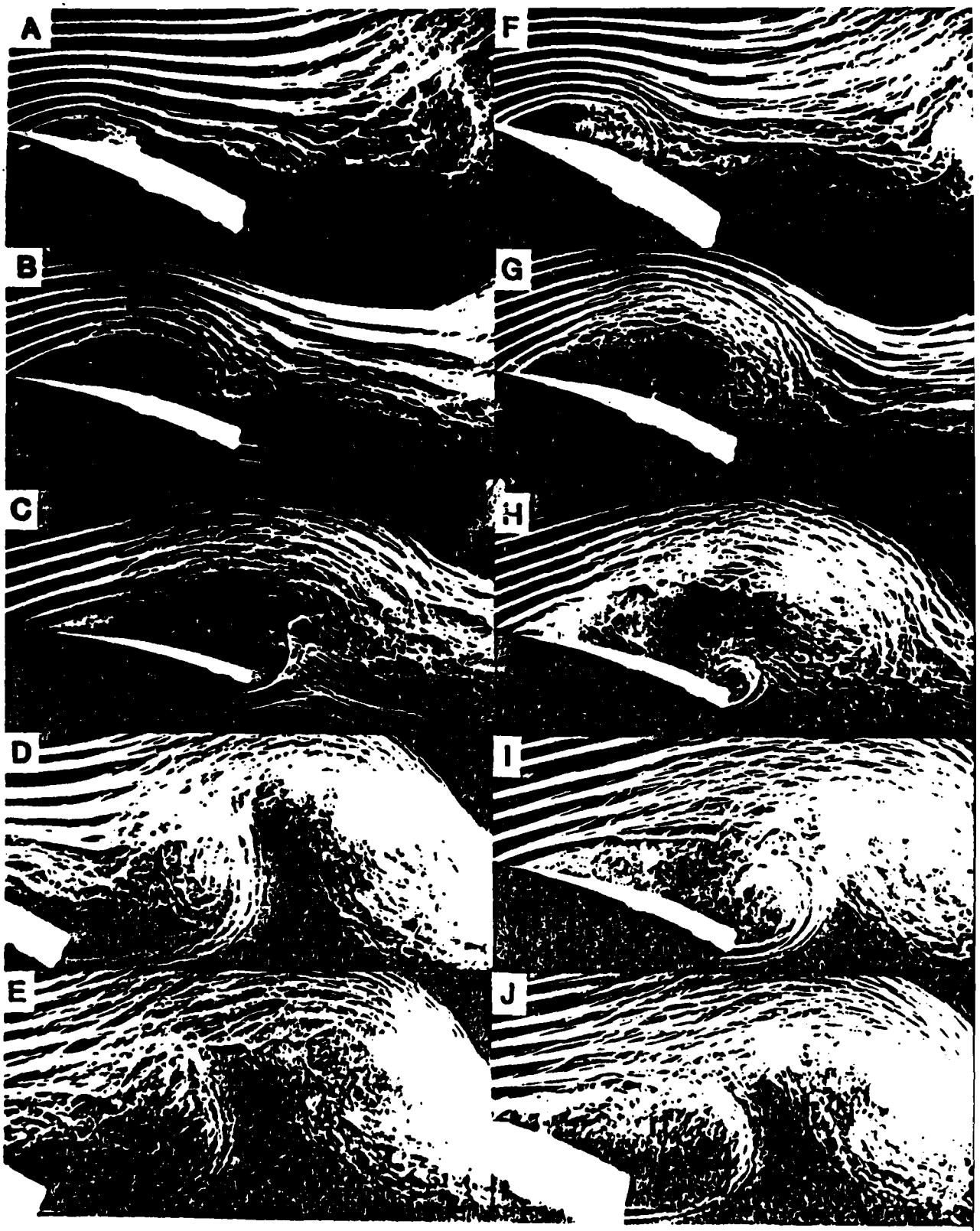
A
B
C
D
E
F
G
H
I
J

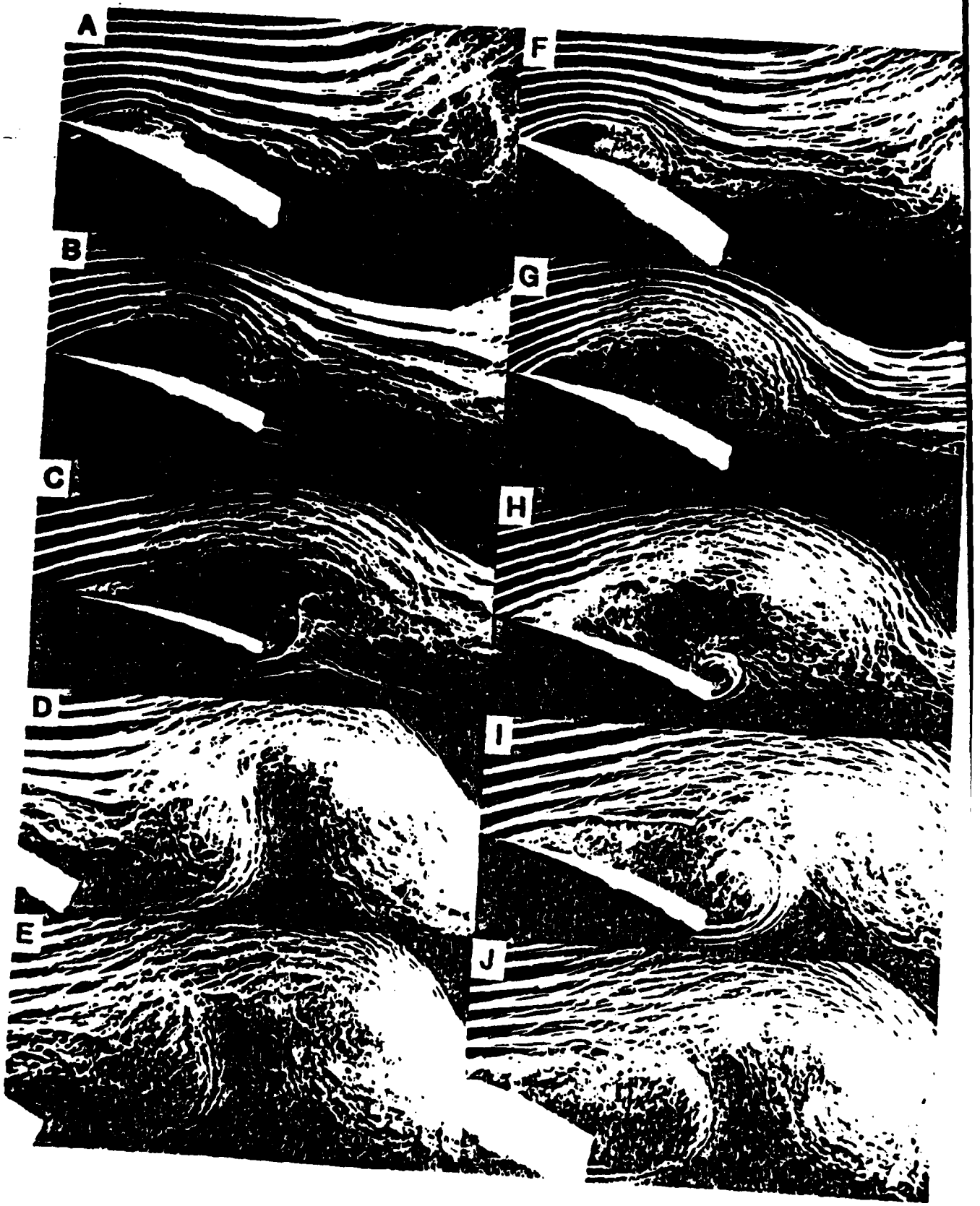
A
B
C
D
E
F
G
H
I
J

E - The combined tandem structure of leading edge and trailing edge vorticity remained cohesive and was visualized many chord diameters downstream of the airfoil.

F - At a mean angle of 20^{o}, a vortex structure was observed forming at the leading edge as the airfoil reached the maximum angle of attack.

G - This vortex was larger than that observed in plate A above. As the vortex traveled to midchord, a rapid growth occurred and was coupled with a strong bending of the streamlines of the surrounding flow field toward the airfoil surface.

H-J - This remaining series documents the trailing edge vortical development. Note that the bending of streamlines throughout these visualizations is enhanced compared to the $15^{o} \pm 5^{o}$ tests. In H a small trailing edge vortex was generated as the leading edge vortex passed the trailing edge. The trailing edge vortex rapidly grew in size (I) resulting in complete flow separation. J shows the interaction of the leading and trailing edge vorticity.

Though these series document two separate sets of test conditions, the same pattern of vortical development emerged. Very little qualitative difference could be seen in the development patterns following changes in mean angles of attack. In fact, at reduced values of K ($K \leq .75$) these patterns of vortical development were evident across a broad set of experimental conditions. Only modest variations in vortical strength were evident.

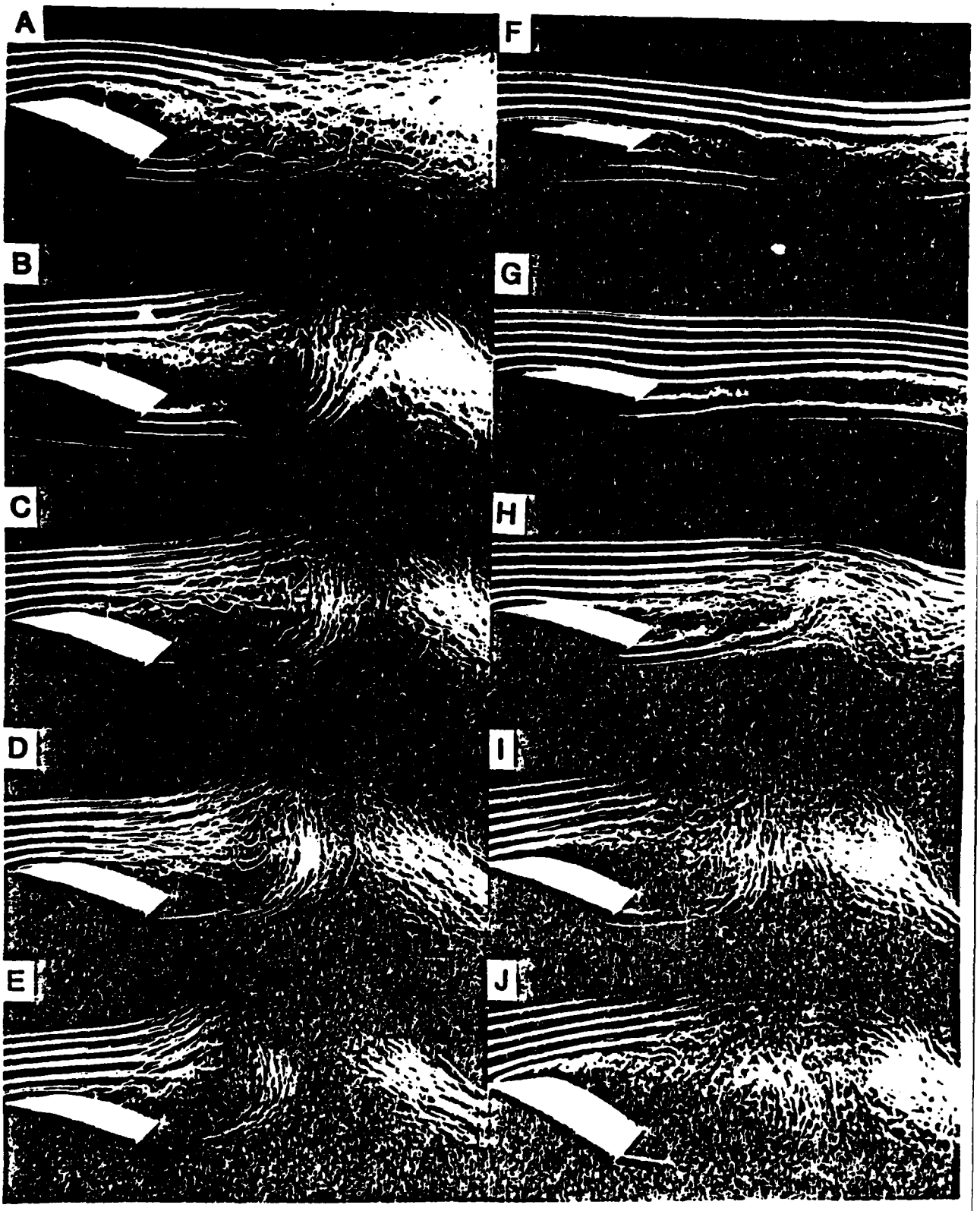
A
B
C
D
E
F
G
H
I
J

Fig. 2 - Flow fields elicited by oscillation angle α_ω and mean angle of attack α_m

These multiple exposure photographs document the changes in dynamic, oscillation-dependent parameter α_ω with variations of the static parameter, α_m. Photographs A-E (≈ 15 phase-locked exposures) were obtained as the oscillation angle was increased from $\pm 1^\circ$ to $\pm 5^\circ$. All other variables were held constant (Re 60,000, K = 0.5, $\alpha_m = 15^\circ$). Photographs F-J were obtained as the mean angle of attack was increased from 0° to 30°. As before, other variables were maintained (Re 60,000, K = 0.5 and $\alpha_\omega = \pm 5^\circ$). Empahsis is placed upon wake structure since both leading and trailing edge vortices are observable at these points spatially and temporally.

Plate

A - At $\pm 1^\circ$ very little synchronus vortical development was evident in the wake structure. The flow field appeared turbulent since superimposition of the streamlines rarely occurred with multiple repeated exposures. Separation of flow occurs over most of the airfoil surface.

B - At $\pm 2^\circ$ both leading edge and trailing edge vorticity was observed. A slight lack of spatial and temporal repeatability of induced structure was evident by the presence of turbulent separation over the downstream half of the airfoil chord.

C & D - With further increases in the oscillation amplitude ($\pm 3^\circ$ and $\pm 4^\circ$), the individual stream lines exhibited more superimposition and the turbulence decreased. Hence, the elicited vortex structure became more temporally and spatially synchronus with the increases in airfoil oscillation amplitude. Flow separation on the airfoil surface was negligible.

E - At $\pm 5^\circ$, excellent temporal and spatial repeatability is obtained. The streamline convergence indicated a well-organized leading and trailing edge vortical interaction in the wake. Again, flow separation was minimal.

F & G - At α_m equal to 0° and 5°, no leading edge vortex development was present in the wake structure. The flow remained attached through the complete oscillation cycle. Vortical flow structures were produced at the trailing edge of the airfoil at 0° and the resulting wake structure was similar to a Karman Vortex Street. The frequency of the wake structure appeared to depend on the airfoil oscillation rate. Small vortices alternately

shed from the boundary layers of the upper and lower surface (180° out-of-phase) produced the observed vortex street. These and all subsequent photographs in this series were obtained with Re 60,000, K = 0.5, and $\alpha_\omega = \pm 5^\circ$.

H - At $\alpha_m = 10^\circ$, a small leading and trailing edge vortical interaction was seen in the wake structure. Under these test conditions, the static stall angle was exceeded by approximately two degrees during the maximum α of the oscillatory cycle. Until the static stall angle was exceeded, vortical development from the leading edge was not seen. The induced structures were relatively weak in appearance, both in the wake and over the airfoil surface.

I & J - At both 20° and 30°, the fully-developed leading and trailing edge vortical interactions were evident. Angles in excess of 15° provided little overall change in the induced flow structure interactions. At this phase of the oscillatory cycle, flow separation, if it is going to occur, is most accentuated. Note that turbulent separation is apparent only at $\alpha_m = 30^\circ$.

In general, increases in the dynamic parameter of oscillation angle increased both the temporal and spatial synchrony of the elicited vortical structure. For the static parameter of mean angle α_m, it was necessary to exceed the static stall angle at some phase of the oscillation cycle in order to generate a leading edge vortex. At mean angles in excess of 15°, few overall differences were observed in vortical development with further increases of α_m. The temporal and spatial synchrony of the vortex structure appeared constant with increases in the mean angle. Whereas the dynamic parameter directly affected the cohesiveness and synchrony of elicited flow structures, the static parameter had little affect beyond the "threshold" or static stall condition.

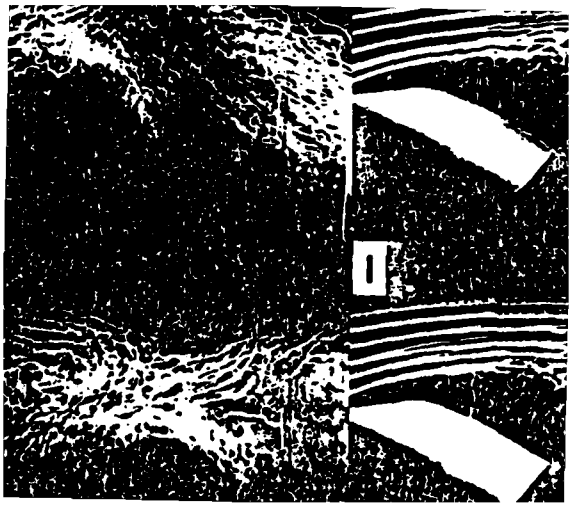

Fig. 3 - Effects of Oscillation Rate (reduced frequency K) and Reynolds Number

These visualizations focus on the effects of the dynamic parameter of oscillation frequency ($\alpha\omega$) and upon Reynolds number. Photographs A-E were made using fixed test conditions of Re 75,000, $\alpha m = 15^{o}$, $\alpha\omega = \pm 5^{o}$. The reduced frequency parameter, K, was increased from 0.25 to 1.75 (1.6 to 11.1 Hz, respectively). All photographs in the sequence were taken at the maximum angle of attack of the oscillatory cycle. Photographs F-J were made at a constant oscillatory frequency of 4.5 Hz, $\alpha m = 15^{o}$ and $\alpha\omega = \pm 5^{o}$ while the Reynolds number was increased from 60,000 to 140,000.

Plate

A - At a reduced frequency of K = 0.25, the leading edge vortex was evident above the trailing edge of the airfoil. The lack of streamline definition as well as vortex definition indicates a relatively weak vortical generation condition.

B - At K = 0.5, leading edge vortex formation was clearly obtained on the airfoil surface. The superimposition of vortical generation streamlines across multiple oscillations is indicative of the temporal and spatial synchrony of the structure. The flow, separated from the airfoil surface by the vortex is bent toward the trailing edge of the airfoil.

C - At K = 1.0, two sets of vortical structures from two successive oscillation cycles are evident in the visualized flow field. One vortex is located at the leading edge while vortices from leading and trailing edges show interactions in the wake immediately behind the airfoil. As K is increased, the separation distance between such successive vortical structures is reduced.

D - With K = 1.5, a leading edge vortex is evident as well as the preceding vortex generated from the previous cycle. The second vortex is located over the trailing edge. Most previous photographs were obtained in phase with the maximum angle of attack. It appeared from examination of the sequences using K > 1.0 that the elicitation of the leading edge vortex occurred at earlier periods in the oscillatory cycle. The acceleration in vort generation was coincident with test conditions that yielded vortex interactions at the trailing edge at the same time that vorticity usually formed at the leading edge.

E - At K - 1.75, two distinctive vortices were clearly resident on the airfoil surface. The formation of the first was about the leading edge and the

second was located upstream of the trailing edge over the airfoil surface. A third vortical interaction was located in the wake just downstream of the trailing edge. This formation was dominated by the trailing edge vortex. Finally, the large leading and trailing edge vortex interaction was fully developed approximately two chord lengths downstream. Thus, as K was increased, the cohesiveness of the streamlines related to vortical development similarly increased. Vortex development became more synchronus with airfoil oscillation. In addition, vorticity generated at the higher K values exerted a more accentuated distortional effect to the surrounding flow field.

F - At a Reynolds number of 60,000, a strong leading and trailing edge vortical interaction occurred. The oscillation rate (4.5 Hz) corresponded to a reduced frequency of K = 0.5 where good synchrony of vortical development was common.

G - At a Reynolds number of 80,000, the oscillation frequency of 4.5 Hz corresponded to a reduced frequency parameter of K = 0.37. The size of the vortical interaction was reduced, yet a good synchrony of developed structure was evident. Both leading and trailing edge vorticity was seen with flow separation from the airfoil surface.

H - At Re 100,000 only a slight vortical interaction was seen in the wake. The scatter of streamlines indicated a poor synchrony of flow with airfoil oscillation. At an oscillation rate of 4.5 Hz, the reduced frequency parameter was equal to 0.3. At lower Reynolds numbers and reduced frequencies (Ref. photo A 75,000, K = .25) considerably more developed flow structure was in evidence. Therefore, this and subsequent photographs indicate that at lower K values, the reduced frequency alone does not fully characterize vortical development. The magnitude of both Reynolds number and reduced frequency, K, play an important role in vortical formation when $K < 0.25 - 0.3$.

I-J - At increased Reynolds numbers of 120,000 and 140,000 (oscillation rate, 4.5 Hz) poor vortical synchrony occurred with airfoil oscillation. These Reynolds numbers corresponded to reduced frequencies of K = 0.25 and K = 0.21, respectively. It must be reiterated that at lower Reynolds numbers with equal reduced frequencies (photo A) synchronous vortical flow structure interactions had occurred. Increases in Reynolds number seemed to reduce

vortical development at lower K values ($K \leq .5$).

Increases in the dynamic parameter, oscillation rate, increased the spatial and temporal synchrony of the generated vortices with any phase of airfoil oscillation cycle. As the reduced frequency was increased, the mean distance between successively generated vortices decreased. As the number of vortices located in the airfoil surface was increased, a greater influence was seen both on the surrounding flow field and amongst the vortices. Increased Reynolds number had the reverse effect. Increases apparently reduced the overall synchrony of vortical development. Under test conditions where the reduced frequency, K, was held constant (Re 75,000, K = .25 cf., Fig. A and Re 120,000, K = .25 cf., Fig. I) increases in the Reynolds number were correlated with decreased vortex generation.

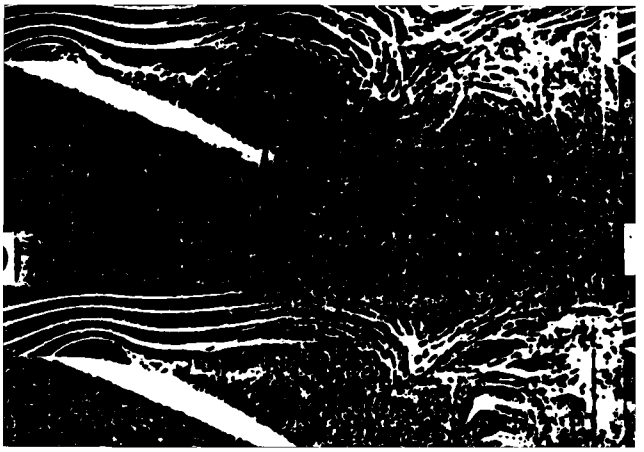

Fig. 4 - Effects of Airfoil Geometry on Vortical Development

This series of multiple exposure photographs examined the sensitivity of vortex development to radical changes in airfoil geometry and test geometry. Figures A - E were obtained using a NACA 0012 airfoil at Reynolds number 60,000, $\alpha_m = 15^o$ and $\alpha_\omega = \pm 5^o$. The reduced frequency was increased from K = 1.0 to K = 2.0 in 0.25 increments. Photographs F - J duplicated the test conditions used in photographs in A - E. The NACA 0012 airfoil, however, was rotated 180^o so that the sharp trailing edge under the normal geometry became a sharp leading edge in the reversed geometry tests. Similarly, oscillation which occurred about the 0.25 chord in the normal geometry occurred about the 0.75 chord location in the reversed geometry. The reversal of the airfoil erected a massive change in both the airfoil geometry and the dynamics in oscillation.

Plate

A & F - The vortex generation sequences across the two test geometries were quite similar. A leading edge vortex was present with a leading and trailing edge interaction occurring in the wake. At low values of $K < 0.3$, the development of vortical patterns appeared fairly autonomous from airfoil oscillation regardless of differences in airfoil geometry.

B & G - At a reduced frequency of K = 1.25, some subtle changes in elicited flow structure occur. The vortex over the leading edge was much more intense with the reversed geometry of G compared to B. The streamlines were more distinct and possessed greater curvature in returning to the airfoil surface. Vortical size was approximately the same but G patterns exhibited more apparent strength. In the wake it was clear that the temporal relation of the trailing edge vortex to the leading edge vortex changed dramatically. The phase relation of trailing edge development and interaction with the leading edge vortex will be addressed subsequently.

C & H - As the reduced frequency K was increased to 1.5 the mean distance between consecutive vortices was reduced. The more spatially and temporally synchronus vortex development is clearly evident in the reverse geometry tests. The pattern of flow over the airfoil surface and the mean spacing between vortices remained constant across both normal and reversed geometry tests. The curvature of remote streamlines was most accentuated and reproducible in reverse geometry tests.

D & I - Further increases, K = 1.75 and K = 2.0, led to more synchronus structure
E & J - in both geometries. The synchrony was preserved even in wake structure. As all photographs were obtained at the maximum angle of attack, the initiation of the leading edge vortex in both geometries occurred at earlier periods in the oscillation cycle as the oscillation rate increased. Though a difference existed in the intensity of elicited structures between normal and reversed airfoil geometries, the distance between subsequent vortices and the placement of structure on the airfoil surface did not vary. The temporal relationship between leading and trailing edge vorticity, however, exhibited significant alterations. Also, the relative strengths of these structures appeared more disparate with reversed geometry.

Qualitatively, the generation of leading edge vorticity did not change with airfoil geometry. The same patterns of vortex initiation, successive vortex spacing and vortex placement over the airfoil surface were observed for both test configurations. Quantitatively, there were differences. The leading edge vortex generated by the sharp edge of the reversed airfoil was seen to be more intense. The subsequent growth of that vortex was both temporally and spatially more well synchronized with airfoil oscillation than the vorticity elicited by normal geometry. The generation of the trailing edge vortex and the interaction between the leading and trailing edge vorticity were quite different.

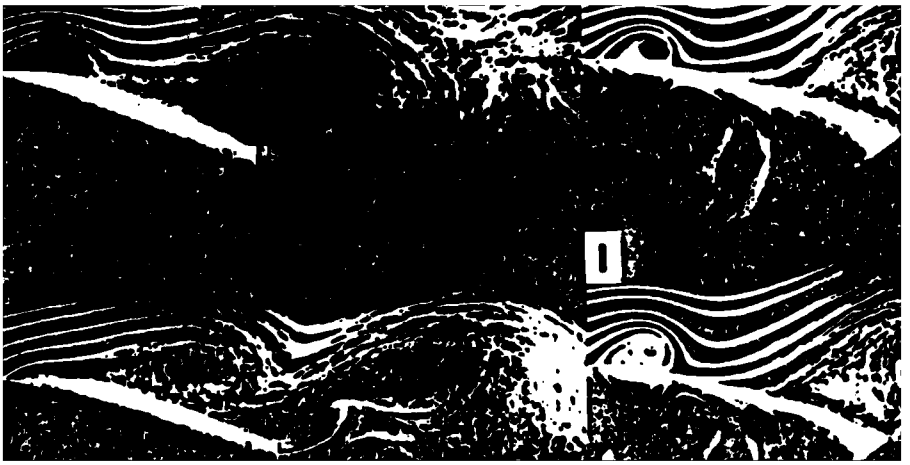

Fig. 5 - Development of the Trailing Edge Vortex: Normal Versus Reversed Geometry

These multiple-exposure photographs were prepared to cite the dependence of vortical development at the trailing edge upon both airfoil oscillation dynamics and reduced frequency parameter. Series A-E used a NACA 0012 airfoil with normal geometry (sharp trailing edge). Photographs F through J were based on 180° reversed geometry (sharp declining edge) using the same airfoil. Both sequences were taken at a Reynolds number = 60,000, α_m = 15° and oscillation angle = ±5°. The reduced frequency, K, was again increased from 1.0 to 2.0 in 0.25 increments. The oscillation angle triggering for the multiple exposures was not maintained at one fixed angle of attack. Rather, the angle was adjusted for each photograph in order to maximize the detail of leading edge-trailing edge interaction in the near field wake just beyond the trailing edge of the airfoil.

Plate

A & F - At K = 1.0, both vortical development of the airfoil surface and generation of the trailing edge vortex are nearly identical. The leading edge vortex passing into the wake of the airfoil either induced or elaborated a trailing edge vortex. The growth of the trailing edge vortex resulted in flow separation over the airfoil. The leading edge vortex is, thus, followed by a trailing edge vortex as a composite, sequential wake structure.

B & G - At K = 1.25, a phase shift has occurred in the normal geometric Fig. B between the passage of the leading edge vortex and the development of the trailing edge vortex. The trailing edge vortex now leads, slightly, the vortex generated from the leading edge into the wake. The influence on flow field separation was also reduced. The leading edge vortex dwells over the airfoil trailing edge during the downstream development of the trailing edge vortex. In Fig. G, the reversed geometry displays a different alteration in flow structure. The trailing edge vortex is generated almost concurrently with passage of the leading edge vortex. However, very little separation about the trailing edge can be seen with the trailing edge vortex generation because this vorticity remains a somewhat weak wake structure.

C & H - At K = 1.5, the trailing edge vortex clearly leads the vortex generated from the leading edge in the normal geometry tests. A large leading edge vortex was centered over the trailing edge with no evidence of trailing edge counter-vorticity beneath it. The trailing edge vortex

can be seen just to the right of the leading edge vortex in the wake. Cataclysmic flow separation is not evident from the airfoil surface. With reversed geometry, the formation of trailing edge vorticity appears suppressed or overwhelmed by the leading edge vorticity. The minimal evidence of trailing edge vortical development occurs at approximately the same chord location with passage of the leading edge vortex. Little evidence existed of flow separation associated with the trailing edge vortex. It appeared that bottom surface, trailing edge flow was simply drawn into the dominant leading edge vorticity. Even the downstream wake structure exhibits evidence for having been drawn into the strong upstream vorticity.

D & E - I & J At the reduced frequencies of K = 1.75 and K - 2.0, the trailing edge vorticity can be seen just downstream of the airfoil trailing edge in the normal geometry of Figures D & E. The trailing edge vorticity clearly precedes the leading edge vortex. These structures continue to exhibit a ordered spatial sequence in the airfoil wake. With the reversed geometries in Figures I and J, the trailing edge vortex occurs in the same chord position with the passage of the leveling edge vortex. Independent sequential wake structures do not occur. Flow separation is no longer evident from the trailing edge vortical development in either geometry. In reversed geometry tests, the strong leading edge vortices compressed into the flow such that they dictate the behavior of less energetic flow elements. It is obvious that the flow between the vortices is held under the strong influences of both upstream and downstream vortex centers.

The foregoing series has established that the pattern of leading edge vortex development is related directly to increasing values of K regardless of test geometry. Yet, development of the trailing edge vortex varies substantially for different geometries as well as different reduced frequencies. Such variations are most notable in the effects seen on leading and trailing edge vortical interactions in the airfoil wake.

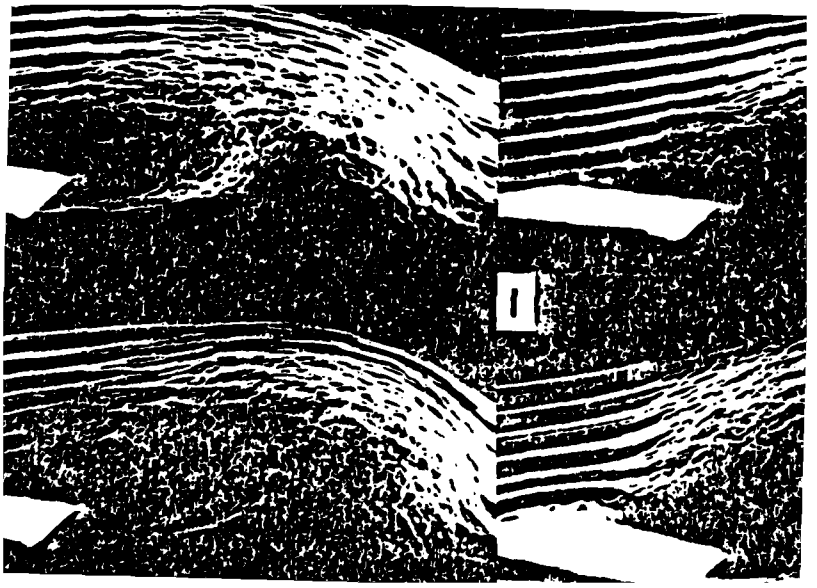

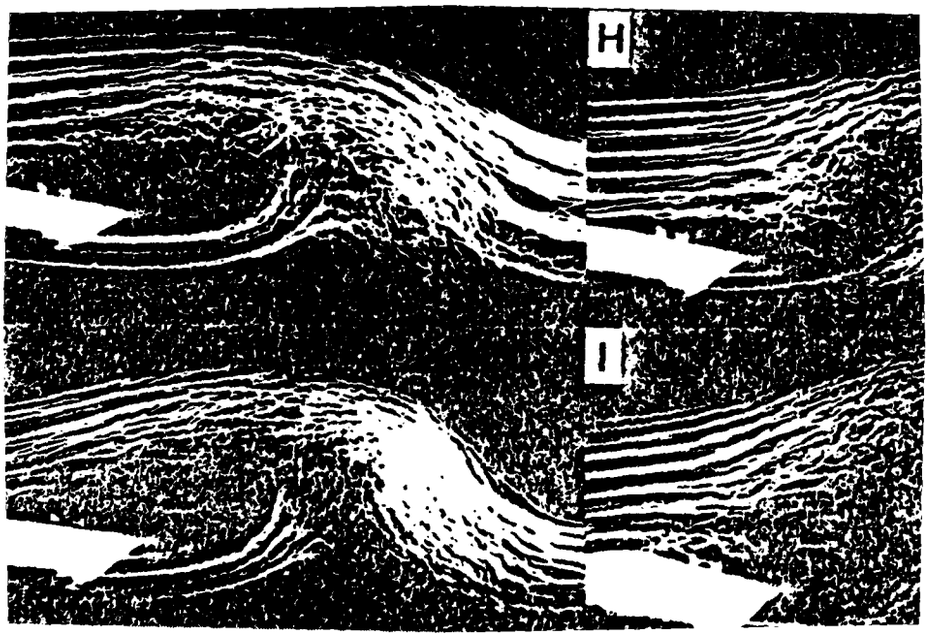
H
I

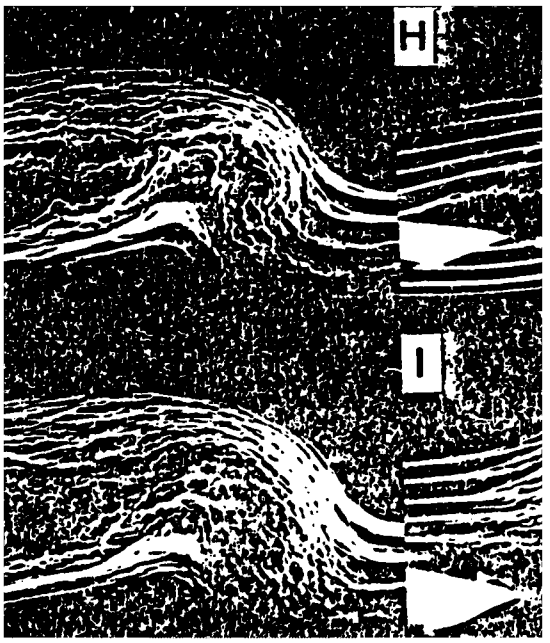
H
I

Fig. 6 - The Flow Structure Exhibited Around a 6' Chord Flat Plate Oscillated at at a variety of angles of attack

Oscillation point at 21% chord. Plates A-E exhibit $\alpha_m = 10^\circ$ and A with $\alpha_\omega = \pm 1^\circ$, B with $\alpha_\omega = \pm 2^\circ$, C with $\alpha_\omega = \pm 3^\circ$, D with $\alpha_\omega = \pm 4^\circ$ and E with $\alpha_\omega = \pm 5^\circ$. All of these visualizations show perturbations for $K = 0.5$. The resulting flow disturbances are proportional to the size of α_ω. The trailing edge vorticity is well-developed in the plate wake and shows progressive increases in leading edge - trailing edge vortical interactions. In these visualizations emphasizing wake interactions, the leading edge vorticity, which is centered just downstream of the trailing edge vortex, continues to produce the major observable flow disturbance. Most critically, the trailing edge vortex continues to produce flow reversal back over the top surface of the airfoil and, accordingly, continues to produce cataclysmic stall conditions at some portion of the oscillatory cycle. In these visualizations, with the plate exhibiting leading edge motion on the down stroke at about mean angles of attack, flow separation is already apparent.

Discussion of Plates F-J will be reserved for later.

Fig. 7 - The Flow Structure Produced by the Conditions Shown in Fig. 6 Except That the Oscillation Pivot Point is Different

Oscillation point at 50% chord. Plates A-E as in Fig. 6. As in the above figure, increases in α_ω result in large flow disturbances as observed in the plate wake. The strength of the vorticity appears to build more rapidly across α when a 50% chord pivot point is utilized. In plates D and E it is clear that the flow line disturbances exhibit pronounced bending not seen in D and E of the previous Fig. The leading and trailing edge vortical interactions in the wake are quite large and are more localized in the streamwise direction. Both vortical structures appear to have preserved symmetries. Flow separation may be somewhat delayed in these experimental conditions.

Discussion of plates F-J will be reserved for later.

Fig. 8 - The Flow Structures Produced by the Conditions Shown in Figs. 6 and 7, Except the Oscillation Pivot Point is Changed

Oscillation point at 79% chord. Plates A-E as in Fig. 6. As in the above two figures, there is an observable increase in vortical size associated with increasing values of α_ω. Overall, however, vortex size changes little with α_ω values of 3°-5°. In addition, leading edge and trailing edge vortices in the


I

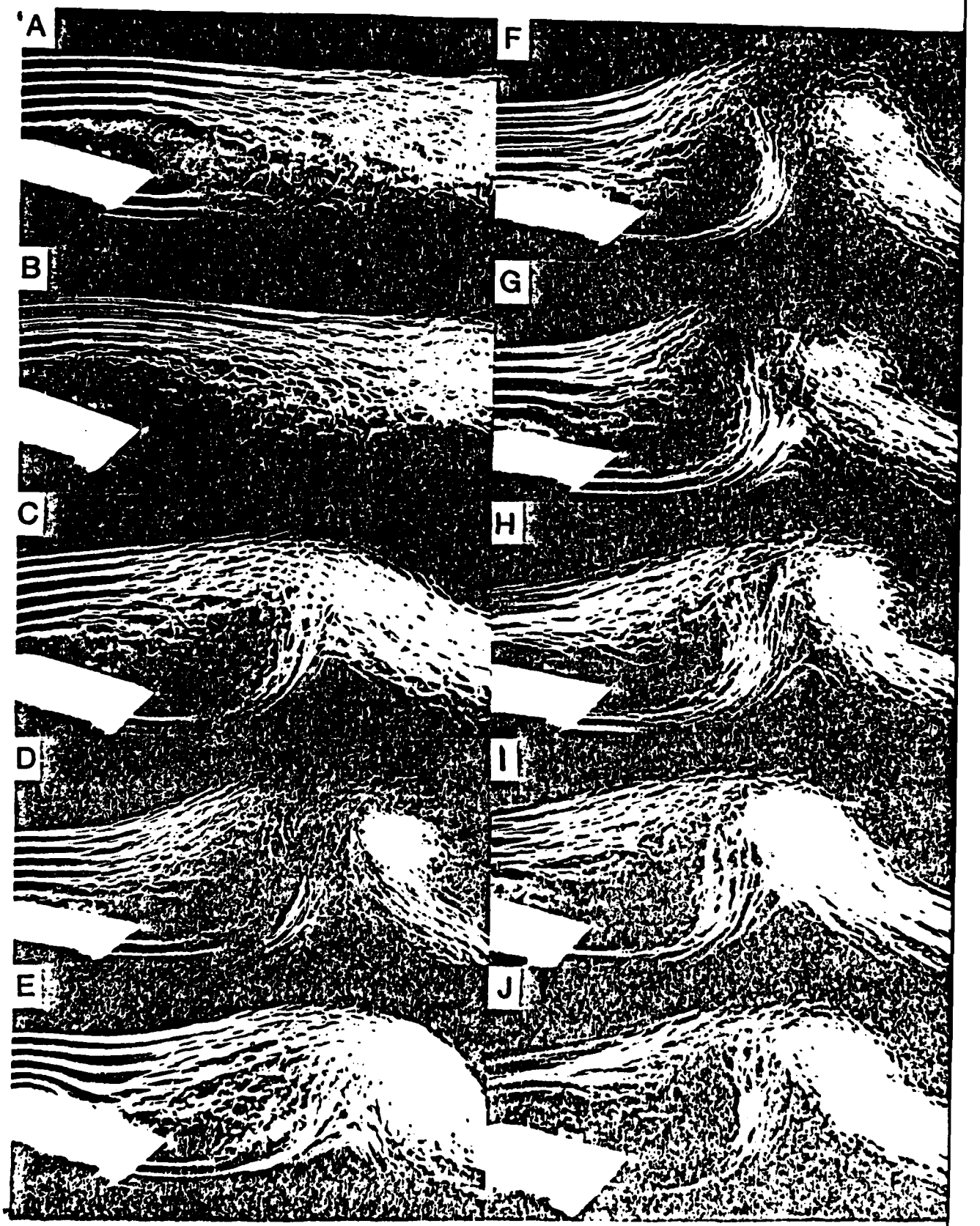
A
B
C
D
E
F
G
H
I
J

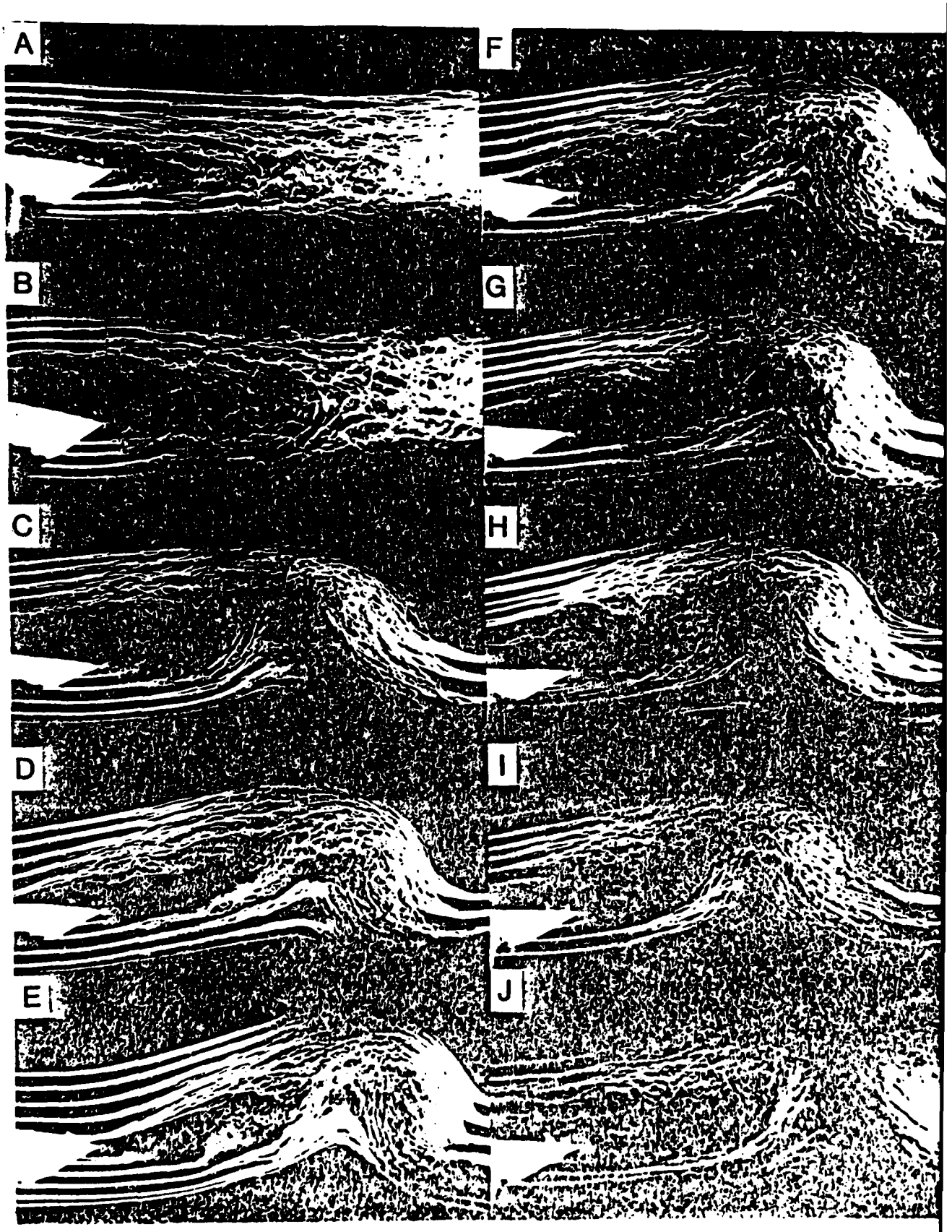
A
B
C
D
E
F
G
H
I
J

wake show reduced interactions compared to the same test conditions except using a 50% chord pivot point. With these particular test conditions and particular oscillatory geometry one might conclude that increases in α_ω beyond $\pm 2^\circ$ result in no additional flow perturbation. This rather surprising finding will be noted in later discussion.

Figs. 6, 7, and 8 - The Flow Structure Induced by Varying α_m and by Altering the Oscillation Pivot Point for the Flat Plate.

In all instances, plates F and G represent α_m of $<\alpha$ stall. The superimposed α_ω of $\pm 5^\circ$ does, however, represent for G plates momentary angle of attack excursions beyond static stall angles during the α_{max} portions of the oscillatory cycle. In Fig. 6, F-J increased α_m values result in large trailing edge vortices which produce striking amounts of flow separation over the downstream portions of the plate. In Fig. 7, F-J the increased α_m values exhibit similar effects except that it is clear the leading and trailing edge vortical interactions are displaced to more downstream portions of the wake. In Fig. 8, F-J with the pivot point at 79% chord the interactions are almost a full chord length downstream. These interactions are both large and well-developed. Surprisingly, however, the flow over the rear of the plate surface is only modestly separated. The other major difference in geometry-induced wake interactions of the vorticity is that Fig. 6 shows clear leading edge vortex definition in the wake prior to trailing edge vorticity positioned upstream. In contrast, Fig. 8 shows stacked vortical interactions in the wake. The leading edge vorticity appears to pass into the wake in a position immediately above the trailing edge vorticity.

Figs. 9, 10, and 11 , Plates A-E - The Flow Structure Induced by a 6" Chord Flat Plate Oscillating in Angle of Attack About Different Pivot Points: The Influence of Increased K Values

In Fig. 9, it is apparent that higher K values tend to generate flow attachment and vortex stacking. The $\alpha_m = 10^\circ$ and $\alpha_\omega = \pm 5^\circ$ conditions appear to require $K > 0.5$ in order to induce flow attachment over most of the plate surface during most of the oscillatory cycle. Except for variations in wake detail for vortex interactions, Figs. 10 and 11 exhibit similar influences for various values of K. It should be noted, however, that allowing the plate to oscillate about the 79% chord position leads to the strongest apparent reattachment and the least

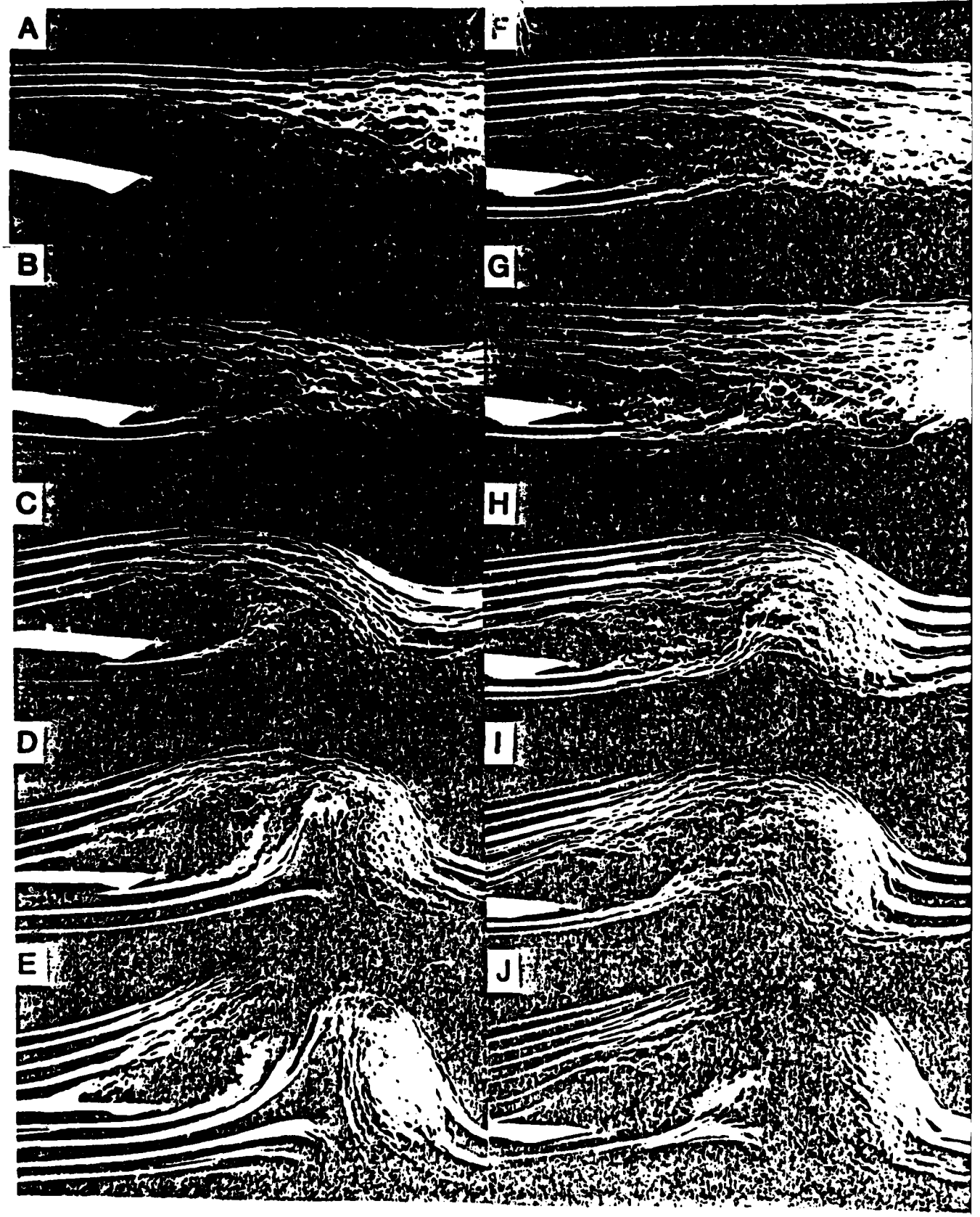
A
B
C
D
E
F
G
H
I
J

turbulent (asynchronous) flow over the plate surface.

Figs. 9, 10, and 11, Plates F-J - The Influence of Re Number on Flow Structures Induced by a Flat Plate Oscillatory About Different Chord Positions.

As may be seen across all plates, Re number has a small negative influence over both reattachment and wake interaction details of the flow. In all cases the $\alpha_m = 10^\circ$ and $\alpha_\omega = \pm 5^\circ$ conditions seem immune to the small changes in Re numbers tested (60,000-100,000).

Fig. 12 - The Influences of Altered α_ω and Pivot Points on the Induced Flow Structure Around an Oscillating 6" Chord Plate.

The $K = 0.5$ and $\alpha_m = 10^\circ$. Plates A-E show pivot point conditions of 21% C and Plates F-J show 79% C. From top to bottom of each sequence α_ω varies from 0°, 1°, 3°, 6° to 9°, respectively, with an Re number of 60,000. The results are quite clear, in that pivot point geometry influenced moderate α_ω flow conditions but not large α_ω conditions. When the values of $\alpha_\omega = \pm 3^\circ$, the pivot point appears relatively unimportant to the flow perturbations elicited by the oscillatory airfoil. As may be seen in plates C-E and H-J, oscillation angle α_ω is also a reasonably weak determinant of flow reattachment. It is, however, a strong determinant of the type and size of wake structure which is to be elicited.

Flow evolution about an oscillating airfoil has been seen to be dependent upon several very powerful experimental parameters: α_m, α_ω, K and Re number. Whereas α_m, α_ω and K combine to yield progressively stronger vortical flows, Re number increments tend to decrease elicited vorticity. Careful studies of flow structures indicate that the stereotyped evolution of a vortex over the surface of an oscillating airfoil may yield to important modifications in the manner in which it interacts with the airfoil and a trailing edge vortex. Such modification can be promoted both by alterations in airfoil geometry and by associated changes in selected oscillatory parameters.

As described earlier (cf., McAllister and Carr, 1978) and refined more recently (Robinson and Luttges, 1983), the upward pitching of an airfoil beyond the static stall angle of attack generates a leading edge vortex. The vortex occurs near the maximum angle of attack and then develops into a large flow perturbation as it passes along the upper airfoil surface toward the trailing edge. Across a wide range of test conditions, the velocity of the vortex movement over the airfoil is approximately 40% free stream velocity. Upon reaching the trailing edge of the airfoil, the leading edge vortex elicits or strengthens a vortex in the flow arising from the bottom surface of the airfoil. This trailing edge vortex, showing flow which rolls upon itself in the upstream direction, has a flow sign opposite to that of the leading edge vortex. In many instances, the growth of this vortex and the proximity of it to the trailing edge of the airfoil resulted in flow reversal over the airfoil surface. The leading edge-trailing edge vortical interactions often caused very rapid flow separation over the airfoil surface involving the full chord of the airfoil. This flow disturbance is consistent with the known

"cataclysmic" flow separation and lift deterioration reported earlier. We have simply documented the causal flow circumstance for this cataclysmic performance change in an oscillating airfoil; it is clear that the trailing edge vorticity is the causal mechanism in question. Finally, in the stereotyped flow circumstance, the trailing edge vortex is shed into the airfoil wake immediately upstream of the leading edge vortex. These side-by-side vortices result in an interaction that produced a localized but strong vertical flow component between the vortical centers. The presence of such vortical interaction, vertical flow "spikes" in the wake of an oscillating airfoil must have significance for rotorcraft but is not the focus of the present discussion.

By extending our experimental parameters, we have determined that critical aspects of the stereotyped flow conditions cited above may be modified. In particular, the leading edge vortex and trailing edge vortex are independent enough that the nature of the interaction of these vortices around the airfoil may be altered and the interaction in the wake may be changed. Since these interactions clearly dictate airfoil lift performance, it is crucial to maximize flow attachment and enhanced lift while minimizing flow separation and stall.

In the present tests it is clear that airfoil geometry and reduced frequency parameter, K, may be altered to virtually eliminate flow separation and stall. As may be seen in the reversed geometry airfoil tests and the $K > 1.5$ conditions, the trailing edge vortices exhibit severely reduced magnitudes and significantly altered phase relations for shedding into the airfoil wake. With a sharp leading airfoil edge pitching upward from the 75% chord position, a very strong vortex is initiated. The vortex remains compact and energetic as it reaches the rounded trailing edge. Because of

vortex strength, the flow over the airfoil, including the vortex itself, remains firmly attached to the airfoil surface. Also, the new oscillatory center for the pitching of the airfoil prevents the trailing edge from exhibiting a significant displacement. Accordingly, the vortex-dominated flow tends to follow the rounded trailing edge curvature toward the bottom airfoil flow. When this vortex-dominated flow is finally shed into the wake, it carries with it the small trailing edge vortex. Leading edge-trailing edge vortical interactions, thus, become exclusively a wake phenomenon. Even in the wake, however, it is clear that the trailing edge vorticity is minimal.

The second means by which to prevent or greatly attenuate separation and stall is to increase K values. Since $K = \omega C/2V_\infty$, values of $K > 1.5$ place two or more well-defined vortices on the top airfoil surface simultaneously These vortices are bounded by the airfoil surface and by the presence of the other vortex. The spatial degrees of freedom remaining for vortical development are few in number. The cohesive strength of the vorticity further limits the flow disturbances possible since the vorticity, to maintain its symmetry, cannot yield asymmetric flow influences. Here the three-dimensional problem clearly arises. However, to date, three dimensional studies are in their infancy and are not particularly useful. Although we do not fully understand the underlying dynamics, it seems certain that high K value tests reveal both vortex-vortex and vortex-airfoil interactions over the airfoil surface. These interactions become stable over the airfoil surface and when these flows are shed into the wake, little surrounding flow disturbance is noted for an appreciable distance downstream. The overall clue to these fortuitous observations is that the vortex-dominated flows on the top airfoil surface establish a dynamic stability before they reach the unbounded flow conditions

at the airfoil trailing edge. To fully understand and quantify these relationships prior to possible exploitation of them in aerodynamic applications, additional, careful parametric tests are needed.

The studies of vortical interactions about an oscillating flat plate will provide some of the needed details. These are discussed elsewhere in this report. And, the potential of our three-dimensional analyses including wing tip vorticity-oscillatory vorticity interactions should complete our understanding of the aforementioned mechanisms.

Oscillating Flat Plate

The generation of vorticity in a zero flow situation was studied using a variety of flat plates driven back and forth at variable rates and stroke lengths. Resulting elicited flow structures were studied following flow visualization photography complemented by low-speed anemometry measures.

When a flat plate is driven into a still fluid, the fluid is displaced ahead of the plate. The displaced fluid also is forced around the edges of the advancing plate to reside in the wake. When the plate is withdrawn from the same fluid element, the displacement occurs in reverse sequence. However, at the end of a stroke the flat plate produces a residual flow which perseveres until the plate completes a cycle and returns to re-energize the flow. Thus, the end of a stroke cycle elicits a flow structure indicative of asymmetric flow generation condition. The manner in which these flow structures are generated, then develop and remain stable is the focus of this report.

Initiation. During the beginning of a plate oscillation sequence, it is possible to observe the progressive building of stable flow structures. Between one to four oscillations are necessary to get to such stability. Such observations suggest that the fluid requires repeated input before full entrainment occurs. The influence of the plate is too weak to initiate the structures which will ultimately persist. Since it is clear that the generated structure deteriorates even within a single stroke cycle, the build-up phenomenon must relate to (1) initiating flow which has a residual effect lasting longer than a single cycle and (2) creating a flow which becomes stable because initiating or maintaining influences equal the deteriorating influences.

Once a stable flow structure is attained, it does not necessarily remain identical throughout the time course of the experiment. In fact, measures obtained anemometrically show a considerable periodicity in some elicited structures. The fixed-point velocity measures show progressive increments in measured velocities through oscillation several cycles and then show a rapid decrease. This modulation influence is continually repeated sometimes exhibiting auto-correlational matches dependent upon 18-25 cycles. Since it appeared that this behavior was not likely to be inherent to the initiation and generation mechanisms, we explored the possibility that "wall-effects" yielded these curious modulations. In changing the test geometry, we found that the modulation of the velocities also varied. We determined, at about the same time, that the flow was not induced in a symmetric fashion. Through several tests of geometry, we determined which effects were germane to the test parameters and which derived from the peculiarities of our apparatus.

GROUP 1

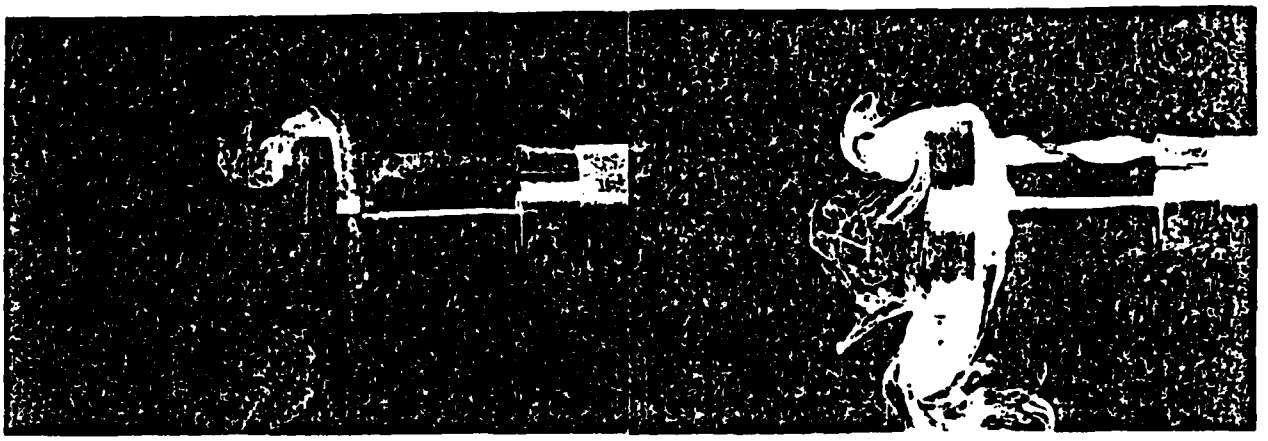

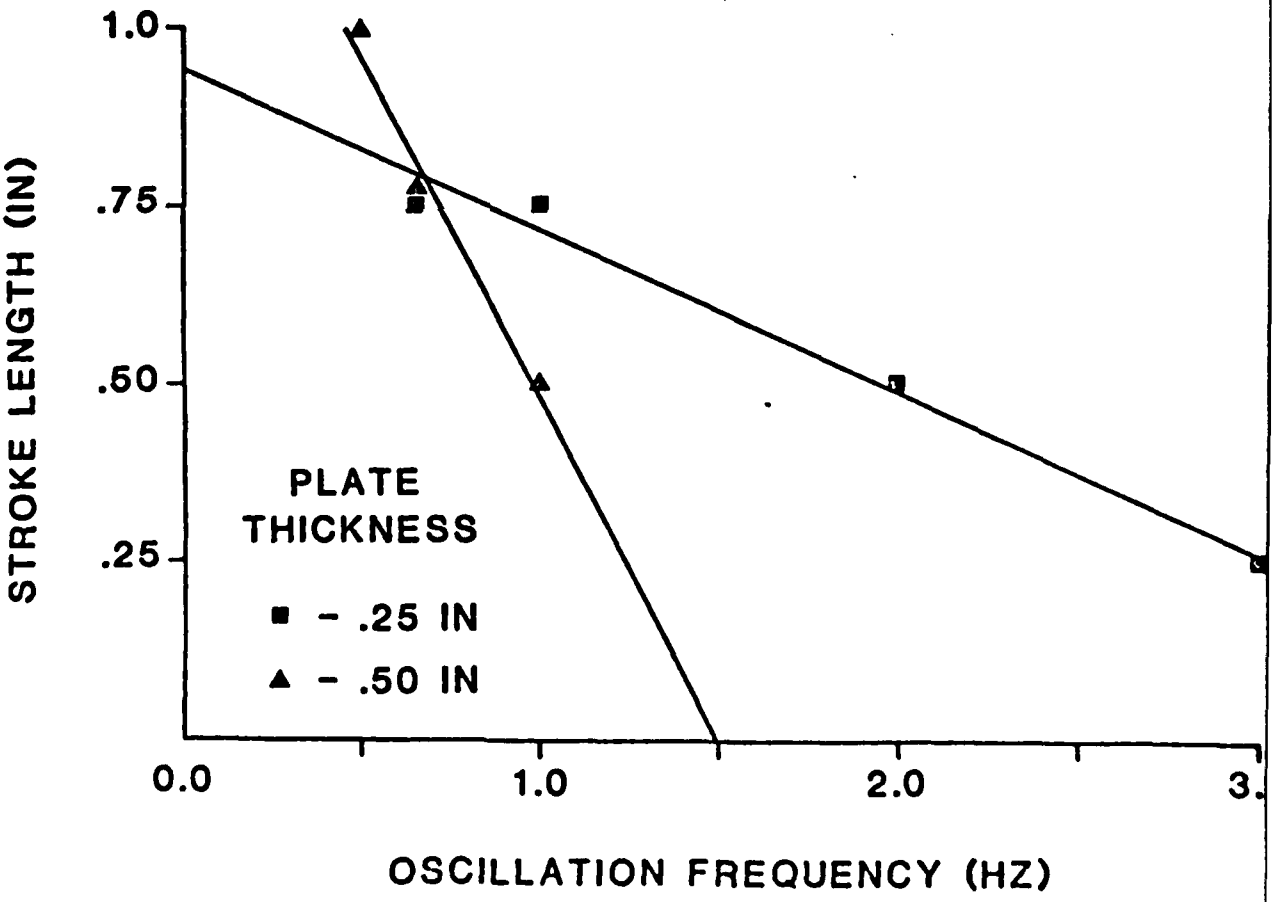
1.0
.75
.50
.25
STROKE LENGTH (IN)
PLATE
THICKNESS
■ - .25 IN
▲ - .50 IN
0.0
1.0
2.0
3.
OSCILLATION FREQUENCY (HZ)

GROUP 2

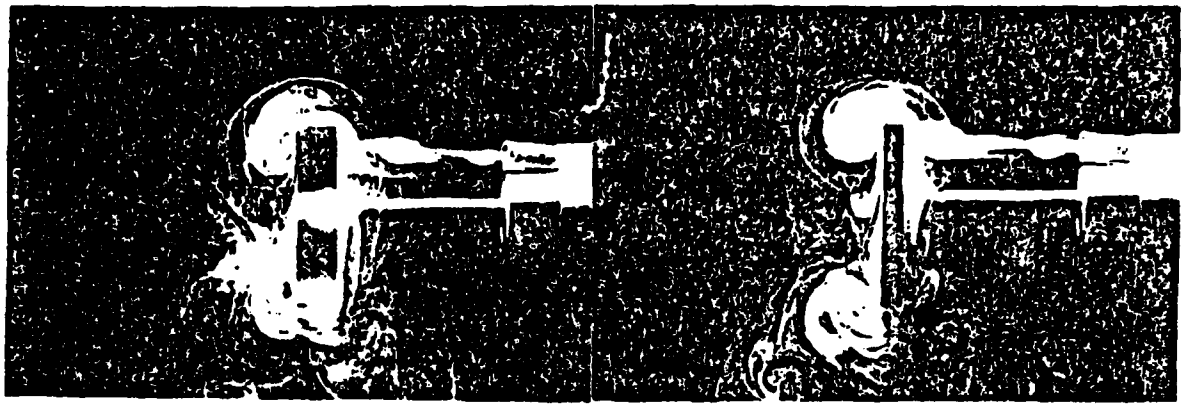

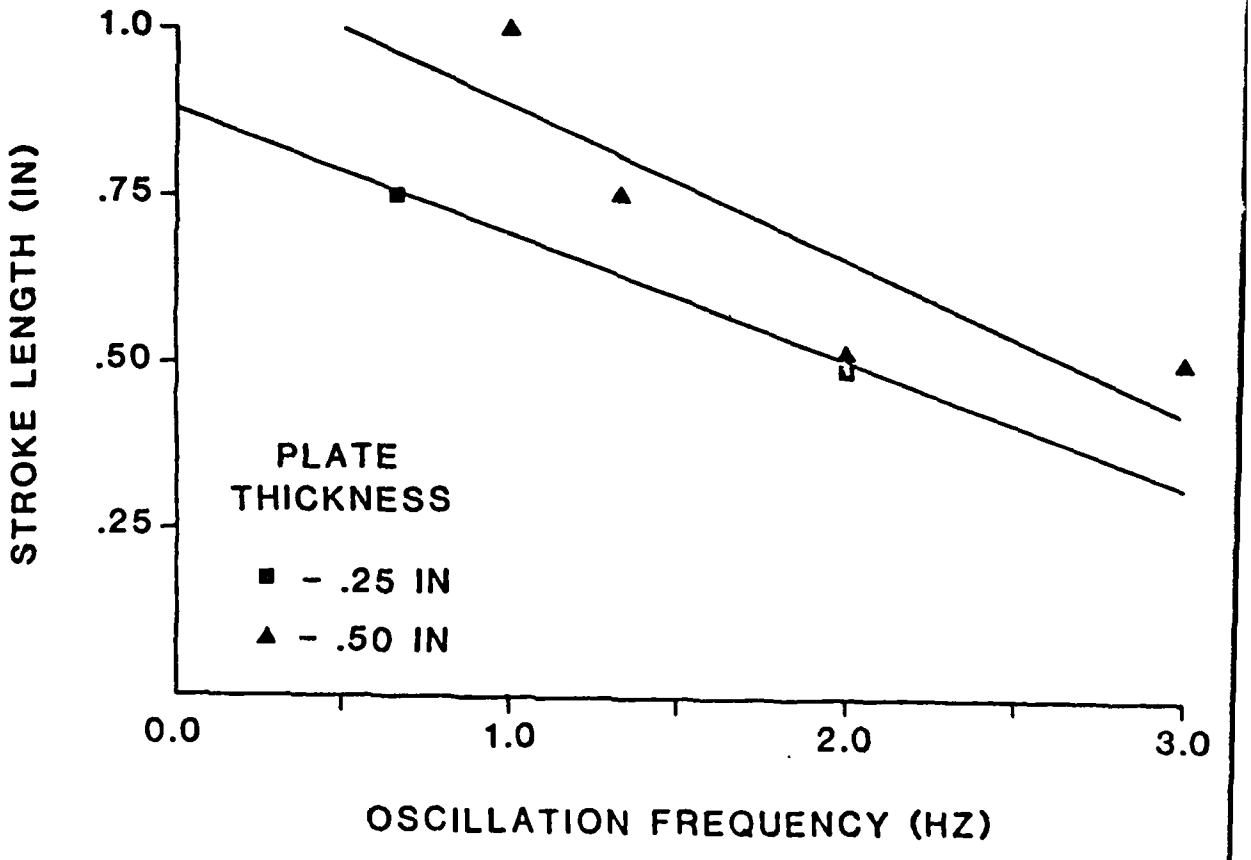
1.0
.75
.50
.25
STROKE LENGTH (IN)
PLATE
THICKNESS
■ - .25 IN
▲ - .50 IN
0.0
1.0
2.0
3.0
OSCILLATION FREQUENCY (HZ)

GROUP 3

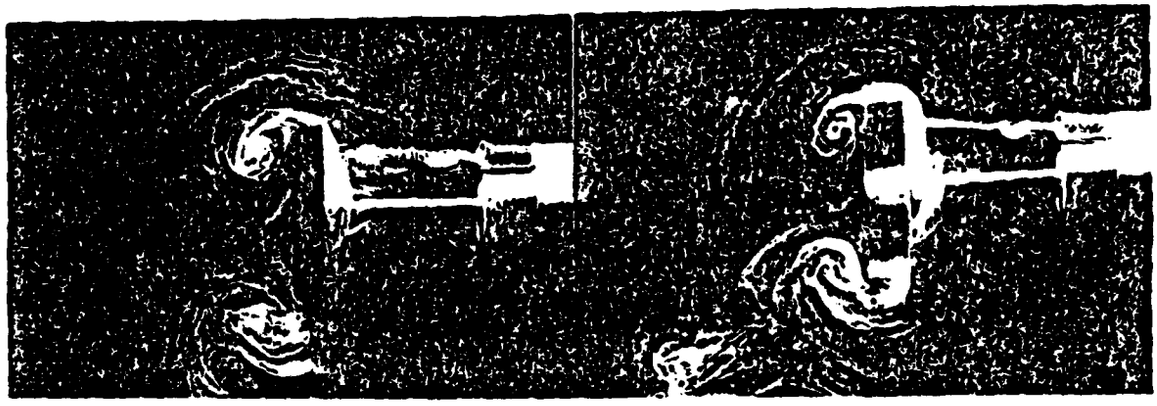

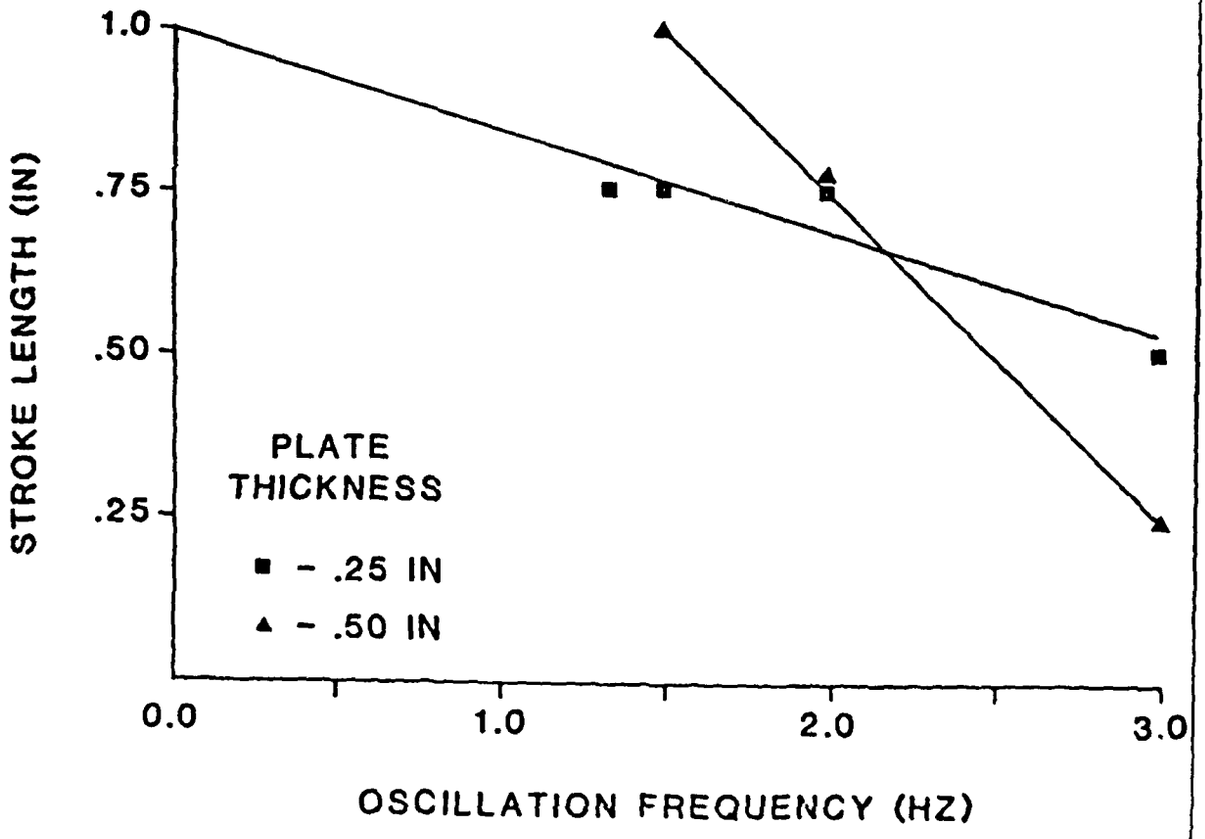
1.0
.75
.50
.25
STROKE LENGTH (IN)
PLATE
THICKNESS
■ - .25 IN
▲ - .50 IN
0.0
1.0
2.0
3.0
OSCILLATION FREQUENCY (HZ)

GROUP 4

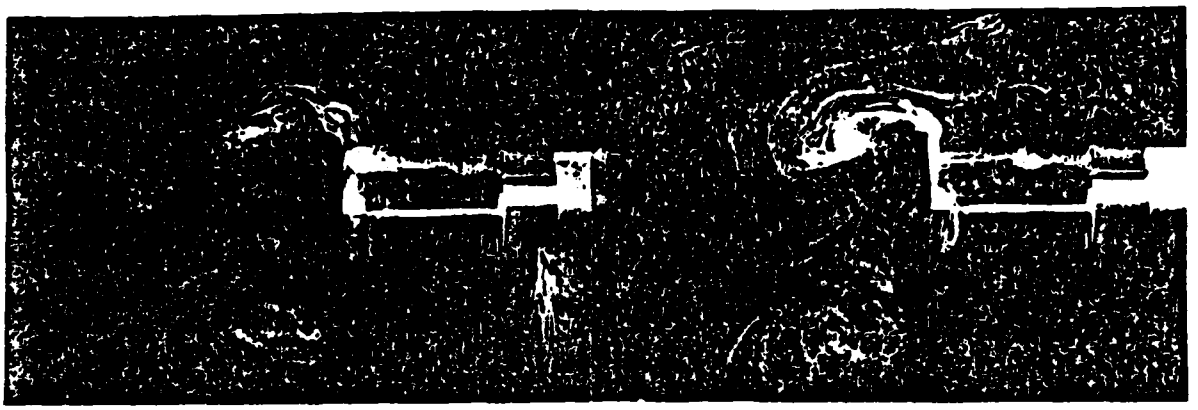

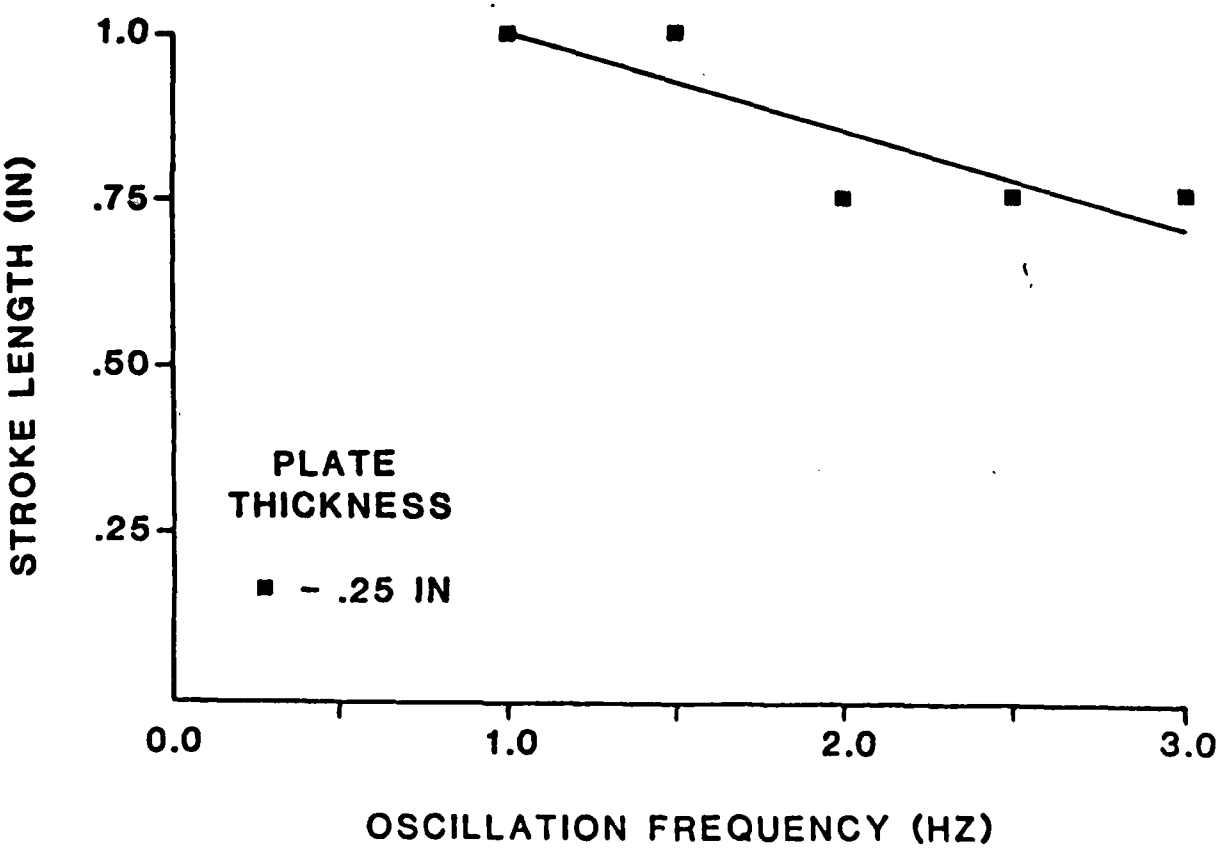
1.0
.75
.50
.25
STROKE LENGTH (IN)
PLATE
THICKNESS
■ - .25 IN
0.0
1.0
2.0
3.0
OSCILLATION FREQUENCY (HZ)

The following data reflect testing in which test apparatus artifacts have been removed or, at least, minimized.

Oscillation of a flat plate in a slow-flow, zero flow environment (90° to flow)

Using flat plates ranging from 1/2, 1/4 and 1/64 inch in thickness, tests were done with each plate driven through a stroke length of 3/4" at 1, 2 or 3 Hz rates. The evolved vorticity exhibited variations in size, strength and proximity to the plate. With no a priori notion of the relationship between either the generation variables or the actual vortical structures elicited the resulting flow structures were simply sorted pictorially by use of a nominal scaling strategy. All photo records were placed into one of six possible groups having the same or nearly the same flow structures. Then, the variables for each were decoded. The resulting selections were plotted in regard to stroke length, stroke frequency and plate size. The results clearly indicated a linear relation between stroke length and stroke frequency. The linear regression line computed for each group had least squares residuals which were very small and had correlation coefficients which ranged from 0.82-0.97. Samples of both the elicited flow structures and the regression lines of flow variables which created them are shown in Figs. 13, 14, 15, and 16. All of these plots are further summarized in Fig. 18.

In Fig. 13, the generation of weak vorticity over the top and bottom of the oscillating plate, at the end of an oscillation cycle is shown. Under appropriate test conditions, both 1/4 and 1/2 in. plates exhibit such vorticity. The most notable facets of these flows are the adjacent weak vortex centers and the obvious movement away from the surface of the plate which generated them. Residual flow from the preceding oscillatory cycle is barely visible. In the case of both test plates, the linear regression on stroke length and oscillation rate is an excellent fit. Whereas large changes in oscillation

rate produce the same flow around the 1/4 inch plate, only modest changes in oscillation rate may be used with a 1/2" plate and still insure the same resulting flows. As might be expected, constant flow perturbations depend upon an inverse relationship between stroke length and oscillation rate.

In Fig.14, the flow parameters elicit vorticity which is considerably stronger than in Fig.13. The resulting vortex center is well-defined, approaching symmetry and is in close proximity to the plate. Spatially, there is surrounding streamline evidence for at least two or three residual flows from previous oscillation cycles. Again, the elicited structure stability is a well-behaved result of a linear regression between stroke length and oscillation rate. Only one experimental point deviates from the regression line and this will be discussed later.

In Fig.15, the resulting vorticity is both well-defined and proximal to the plate surface. The vortices appear displaced from the edge generation site toward the center of the plate. Flow interactions between top and bottom vortices are weak but evident. Also, the residual vortical flow lines from previous stoke vortices perseveres for at least 3-4 stroke cycles. As will be shown subsequently, these residual flow patterns belong to a continuing circulation around the oscillating plate within the zero flow test box. As in previous levels of elicited vorticity, these patterns may be generated across a variety of oscillation rates, plate sizes and stroke lengths. Within any given plate thickness, however, these patterns are generated by a linear relation between increased oscillation rates and decreased stroke cycle.

The flow patterns of Fig.16 are indicative of strong vorticity exhibiting modest amounts of interaction. Vortical flow size, compared to less energetic testing conditions, has increased. The flow between the top and bottom vortices is reasonably strongly entrained and evidence of

flow from previous stroke cycles is far removed from both the plate surface and the present vorticity. Under these test conditions, only the 1/4" plate elicited such strong vorticity. (A separate series of tests with a 1/64" plate will be presented later.) Residual flow from previous stroke cycles is far removed from the strong vorticity visualized under these test conditions. Despite the more complicated flow interactions, the linear regression on the reciprocal relation between stroke length and oscillation rate continues to specify the manner in which these variables combine to elicit the observed flow structure.

In order to determine whether the flow visualizations yielded a reliable and valid index of elicited flow structure, including assumptions of relative velocities, anemometer measures were collected. Using an overheated thermister (1/32" dia.; calibrated against a known reference in an open flow), the velocity profiles corresponding to various positions about a test plate were obtained. In Fig. 17, typical velocity profiles are plotted against the position of the thermister probe over the top of an oscillating 1/4" plate. The probe was moved vertically from the plate in 2 mm increments. The velocity of each point is shown for the stroke cycle phase corresponding to the aforementioned flow visualizations. For further comparison purposes, the stroke length was held constant at 3/4" and the oscillation rate was varied as indicated. Essentially, the velocity profile of the top vortex was measured from vortex center to 4 cm from the center. The results clearly indicate that vortical velocities correspond nicely to observed flow disturbances. The more rapid oscillation rates correspond to larger elicited velocities and to spatially more exaggerated flow disturbances. As might be expected, the spatial decrease in velocity across test conditions is of the same order.

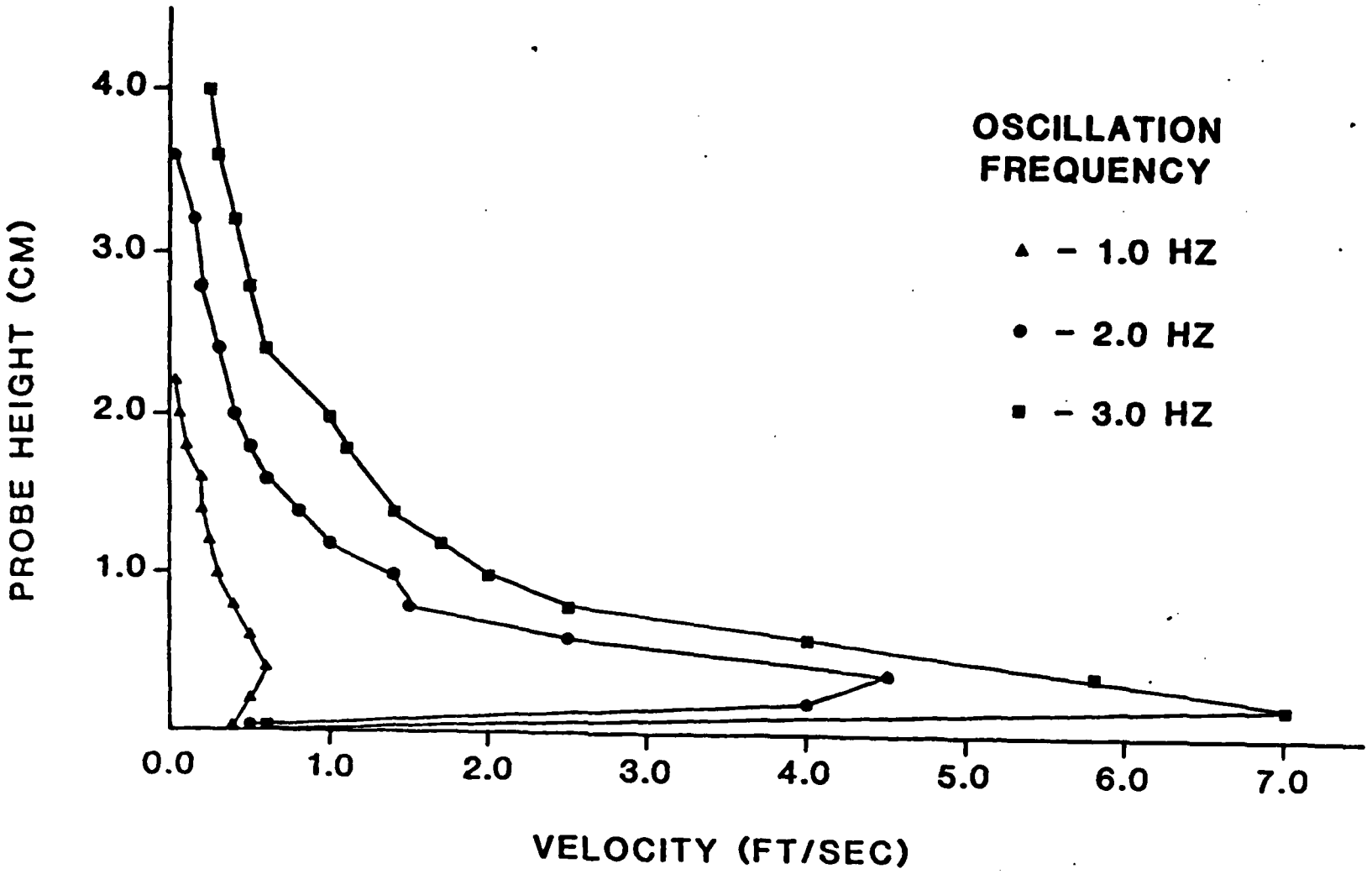
PROBE HEIGHT (CM)
4.0
3.0
2.0
1.0
0.0
1.0
2.0
3.0
4.0
5.0
6.0
7.0
VELOCITY (FT/SEC)
OSCILLATION FREQUENCY
▲ - 1.0 HZ
● - 2.0 HZ
■ - 3.0 HZ

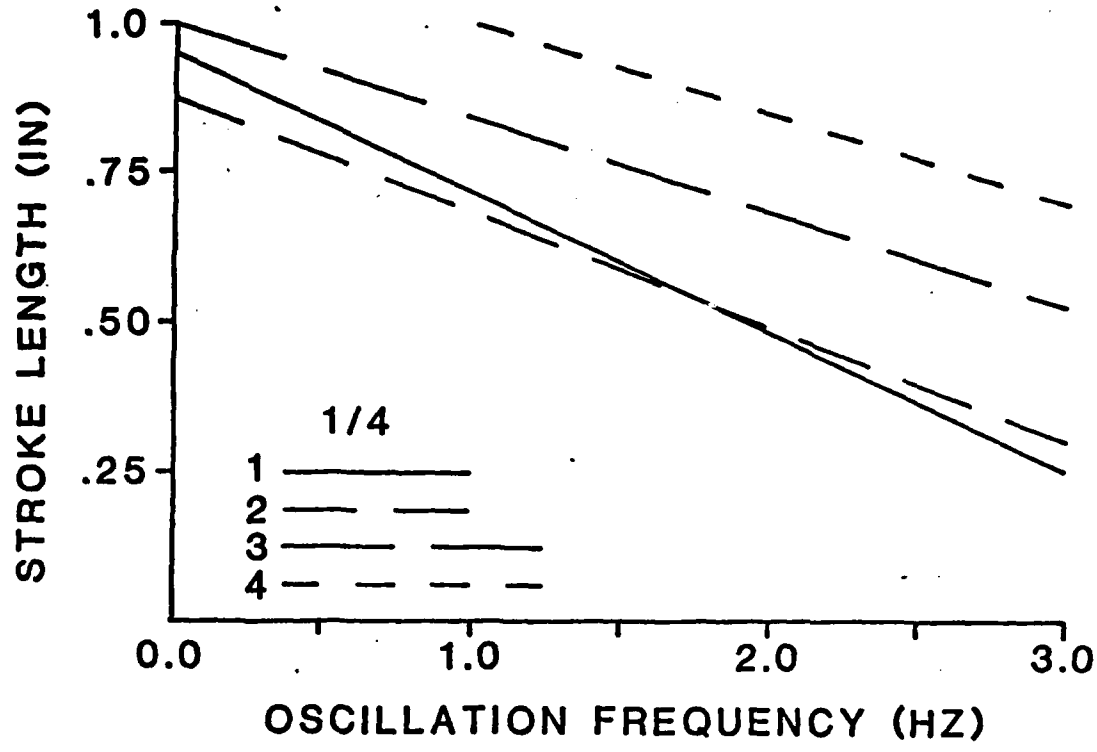
1.0
.75
.50
.25
STROKE LENGTH (IN)
1/4
1
2
3
4
0.0
1.0
2.0
3.0
OSCILLATION FREQUENCY (HZ)

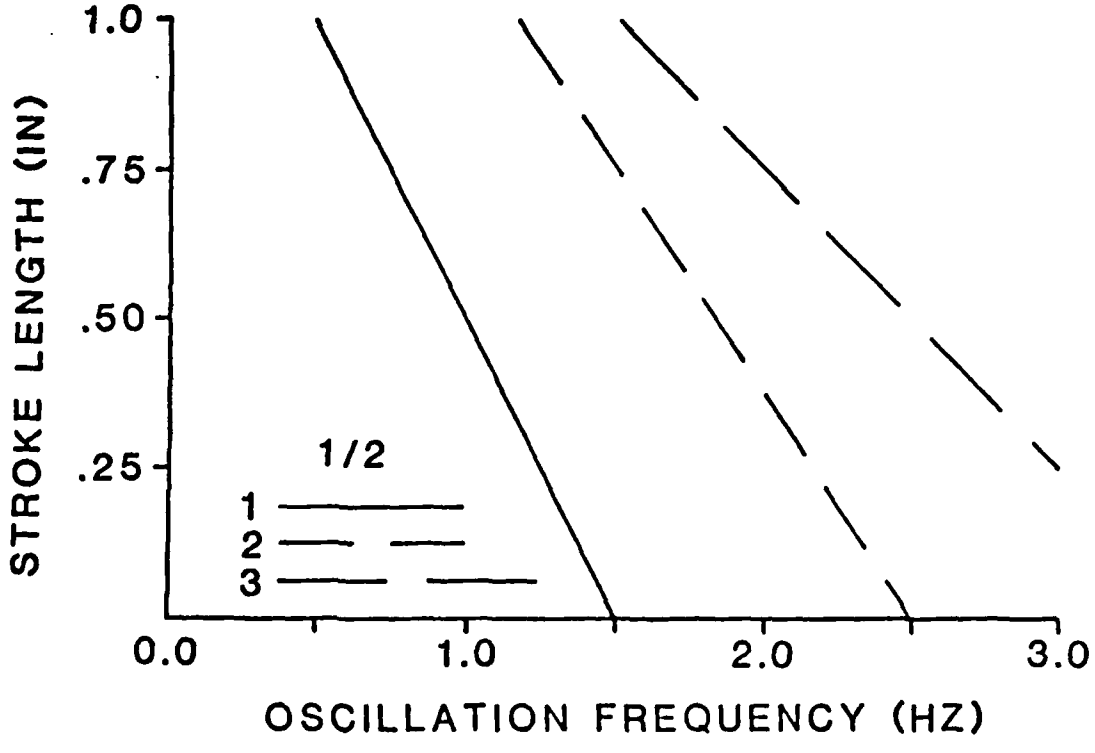
1.0
.75
.50
.25
STROKE LENGTH (IN)
1/2
1
2
3
0.0
1.0
2.0
3.0
OSCILLATION FREQUENCY (HZ)

Having established the validity of the flow visualizations for representing the elicited flow structure, all of the data from Figs. 13-16 were summarized in Fig. 18. In these instances, stronger vorticity (on a hypothetical z-axis) is generally to the upper right of each graph. For the 1/4 in. plate, weak vorticity is obvious for vortical velocity profile maxima $0.3 < x < 1.0$ ft/sec. Moderate but spatially separated vorticity exhibits velocity peaks approximately 1.5 ft/sec. And finally, stronger spatially-interactive vortices are characteristic of velocity maxima > 1.8 ft/sec. The larger thickness plate exhibited similar correlations of flow patterns to velocity profiles.

Two additional observations may be made regarding the data summarized in Fig. 18. The thicker plate yields vortical strength increments dependent upon both stroke length and oscillation rate increments. Overall, this plate produces more increases in vorticity simply dependent upon oscillation rate. In contrast, the thinner plate was clearly more dependent upon stroke length for producing increased vorticity. In order to corroborate these observations, we conducted tests using a 1/64 in. plate having length and width dimensions which were the same as those of the 1/2 and 1/4 in. plate.

The flow visualizations in Fig. 19 summarize the vortical flows induced by a 1/64 in. plate oscillated at 1, 2 and 3 Hz as well as across 1/4, 1/2, 3/4, and 1 in. stroke lengths. From top to bottom of the array of photographs, the stroke length increased. Clearly, the size of the elicited vortical flow is directly proportional to the stroke length. From left to right, the oscillation rate was increased from 1 to 3 Hz. Although some indication of increments in vortical strength is present, this effect of oscillation rate is minimal. It appears that once vorticity has been elicited, additional increments in oscillatory rate may have only minor consequences to

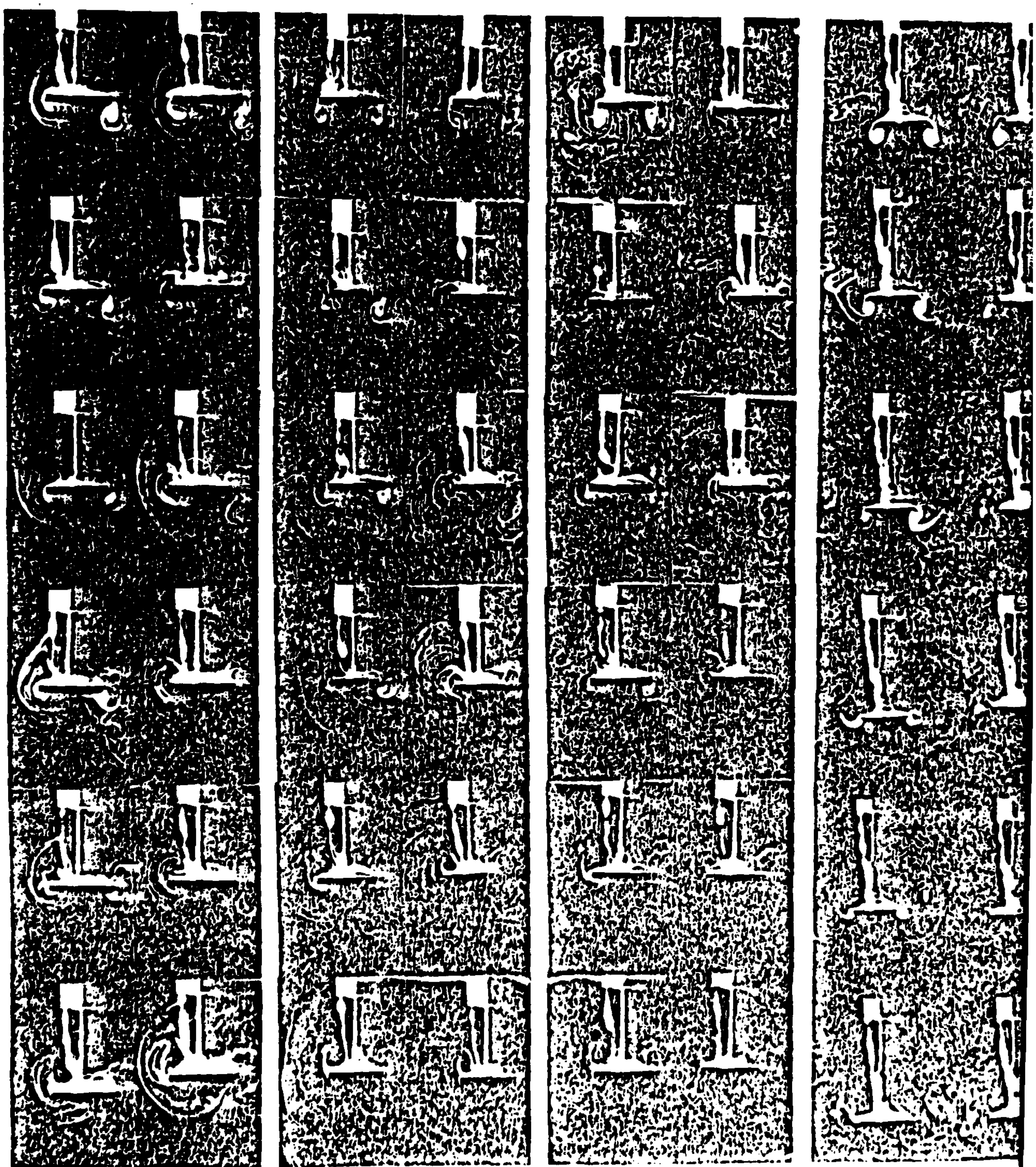

the flow. This observation, of course, could be crucial to the creation and utilization of vorticity in unsteady flows.

When the whole sequence of flow perturbation is visualized from one end of an oscillatory cycle, through 360° and back to the origin, the resulting flow patterns reveal considerable complexity. Samples of such sequences throughout individual oscillatory cycles for different test conditions are shown in Fig. 20. The stroke cycles begin at the left at maximum extension, the plate is pulled to the smoke source for minimum stroke length. The series of visualizations show $\pi/12$ increments through this whole stroke cycle. As might be expected, the flow interactions viewed in this way reveal extremely complex structures. Dominating these structures are the instances of plate direction reversals which lead to vortical formations of opposite sign or directio compared to the existing vorticity. The resulting "stacked" vortical flows show two major states. Small, combined vortices appear to persist in close proximity with each other when none of the vortices are overly energetic. And secondly, with increasing vortical strength the vortices exhibit strong, mutually destructive interactions. Within some instances, therefore, vorticity may exist near centers of opposite direction vorticity and may do so without extensive interaction. In other cases, vorticity of opposite sign appears to "unwrap" vortices of normal flow direction. These latter interactions also appear to lead to an overall flow vector in the direction of the unbounded surrounding fluid: neither toward the vorticity of the bottom edge of the plate nor toward the flow areas directly impacted by plate-induced flow.

From the above observations, it is clear that vortical interactions which are bounded by non-fluid, moving elements and other vortices exhibit several qualitative variations in flow. These different interactive states may be an important clue to the optimal generation and use strategies to be

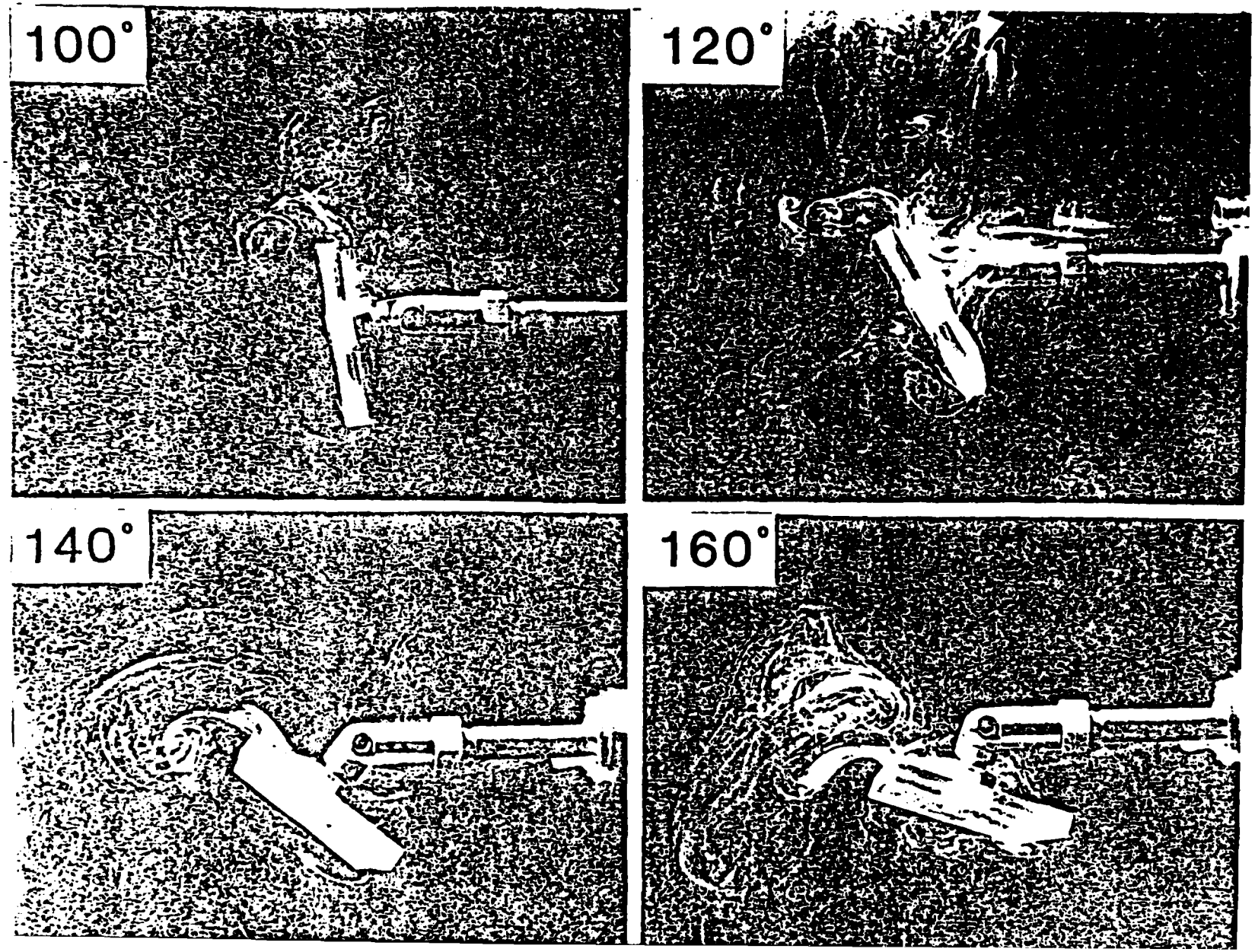
100°
120°
140°
160°

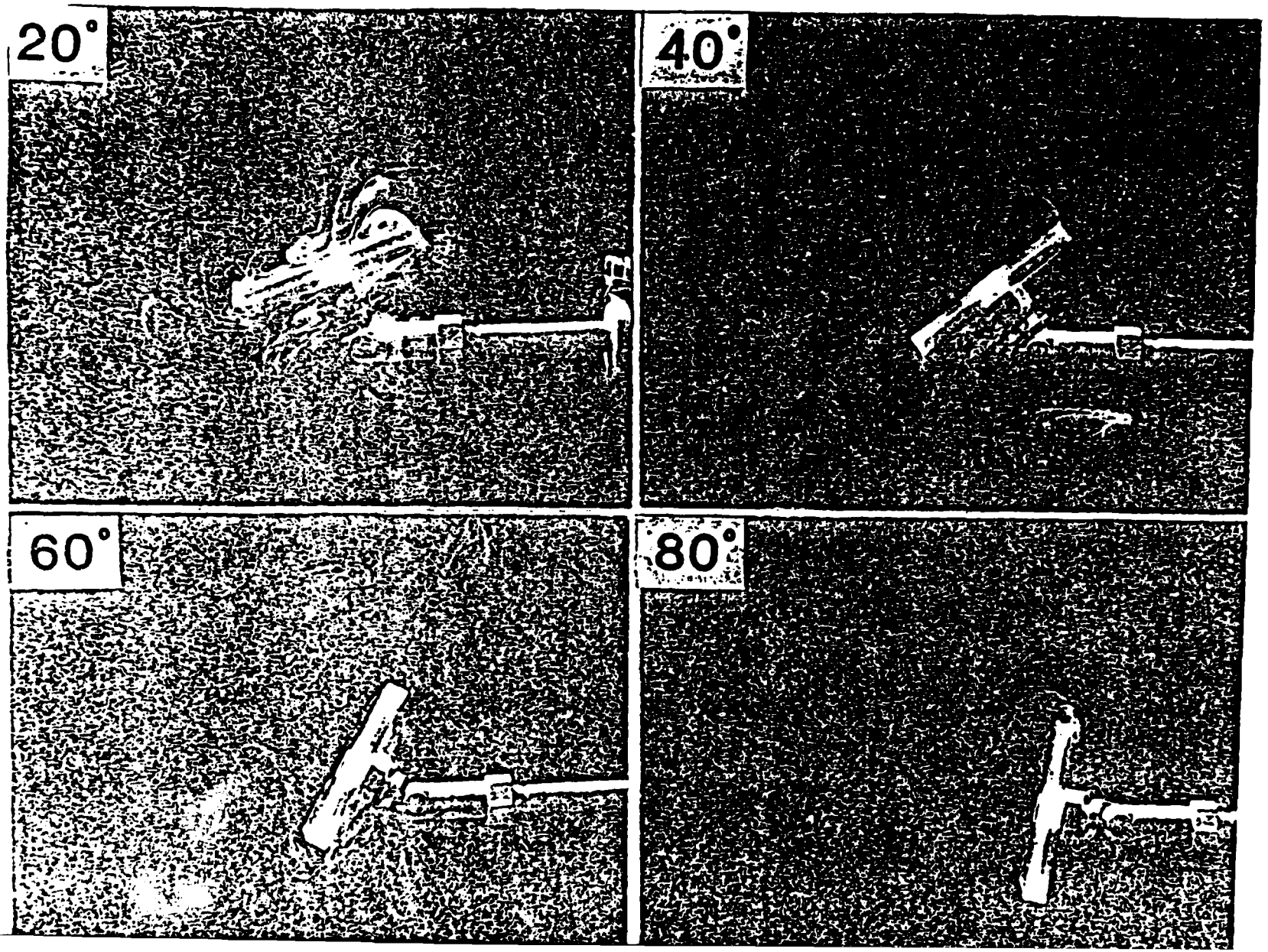
20°
40°
60°
80°

employed for unst[illegible] flows.

Oscillating Flat Plate in Zero-flow, Slow-flow: Altered Angle

Since a portion of our studies of flat plates relates to the modelling of flow around the wings of dragonflies, we have added angularity to the test parameters. In these studies, the elicited vortical flows are simply related to variations in plate orientation relative to plate oscillatory motion. The normal 90° plate orientation is decreased to 20° or increased to 160°. Although the dragonfly (as well as other insects suspected of using the Weis-Fogh pehnomenon) exhibits wing orientations which average a 90° orientation to wing beat direction, variations in this orientation occur due to (1) spanwise twists of the wing and (2) front-back motions incorporated into the path traced by the wing tips during each wing beat cycle.

The flow elicited by a 1/4 in. plate oscillating at 2 Hz across a stroke length of 3/4 in. is summarized in Fig. 21 and Fig. 22. At 20° the elicited vortices stack over the plate surface and the net flow moves ahead of, behind, and straight down from the plate. When the angle of the plate is decreased to 40°-60°, the vorticity is simplified and the net flow is asymmetrically distributed into the surrounding flow field. Finally, at 80° or more the flow again appears to move upward from the top and downward from the bottom edges of the oscillating plate.

Increases in angularity beyond the normal 90° plate orientation result in a similar set of flow interactions. At 100° the elicited vorticity exhibits an organized net flow up and away from the oscillation. The net flow is quite pronounced. At 120° and 140° there is little evidence of a net flow and the vortical interactions are largely mutually disruptive. Finally, at 160° the elicited flow is downward both slightly ahead of plate movement and behind.

What we are beginning to learn from these studies of angularity is that vortical circulation prescribes definite flow possibilities. And these flow possibilities are a complex result of where the vortices are located, both relative to other vortices and unbounded surrounding fluid. Despite the inherent complexity of the plate-induced flows and the net surrounding flow characteristics, many instances of repeated flow patterns exist. These patterns are complex but are far from exhibiting true turbulence. One other point needs to be made here. Since these flows derive from a model of dragonfly induced flow, it seems reasonable that the actual flow interactions exploited by a dragonfly must be spatially stable and predictable. The hovering dragonfly, for example, exhibits extreme spatial precision in the absence of radical wing motion. It seems that position stability, in this example, must derive from extremely stable, predictable wing-flow interactions. This, then, is a benchmark criterion for our work.

Oscillating Wing: Pseudo Three-Dimensional Flow Visualization

Beginning last summer we initiated experiments using an oscillating wing. The wing was constructed from NACA 0015 airfoil stock (6 in. chord) and was fitted with a spanwise blunt but radially rounded wing tip. The oscillatory mechanism permits oscillation rates up to 15 Hz and oscillation angles, α_ω, up to $\pm 25^o$. These dynamic pitching variables may be superimposed upon any fixed angle of attack, α_m.

Flow visualization was achieved in the normal manner (Kodak Tri-X, 800 ASA; 7 μsec. illumination, 35 mm film format). The flow marking source was a smoke wire (0.012 in.) which could be positioned at any location across the span of the wing. Resulting visualization consisted of a planar view of flow across the wing surface and into the wake. A series of spanwise planar views provided a three-dimensionality to the overall flow patterns.

Although the data discussed here represent the most fundamental elements of the results from this experiment, more suitable data synthesis is currently being developed. Using the planar views accumulated from numerous spanwise points, a digitizing pad is used to enter data points into a series of files in our LSI 11/23 system. Each file contains X and Y axis demarcations for each data point. In addition, each file contains a Z reference (span position). Once accumulated, these data arrays are shipped by modem to the Cyber computer. Here the files are reassembled to provide the data points for a three-dimensional graphics representation of the flow about an oscillating wing. Development of this approach should attain fruition in the Spring 1983.

Flow Characteristics at the Wing Tip

Flow around the wing tip exhibited a characteristic twisting from beneath the wing to above the wing as it traveled downstream. This toroidal flow was most well defined in streamlines allowed to pass over the wing tip

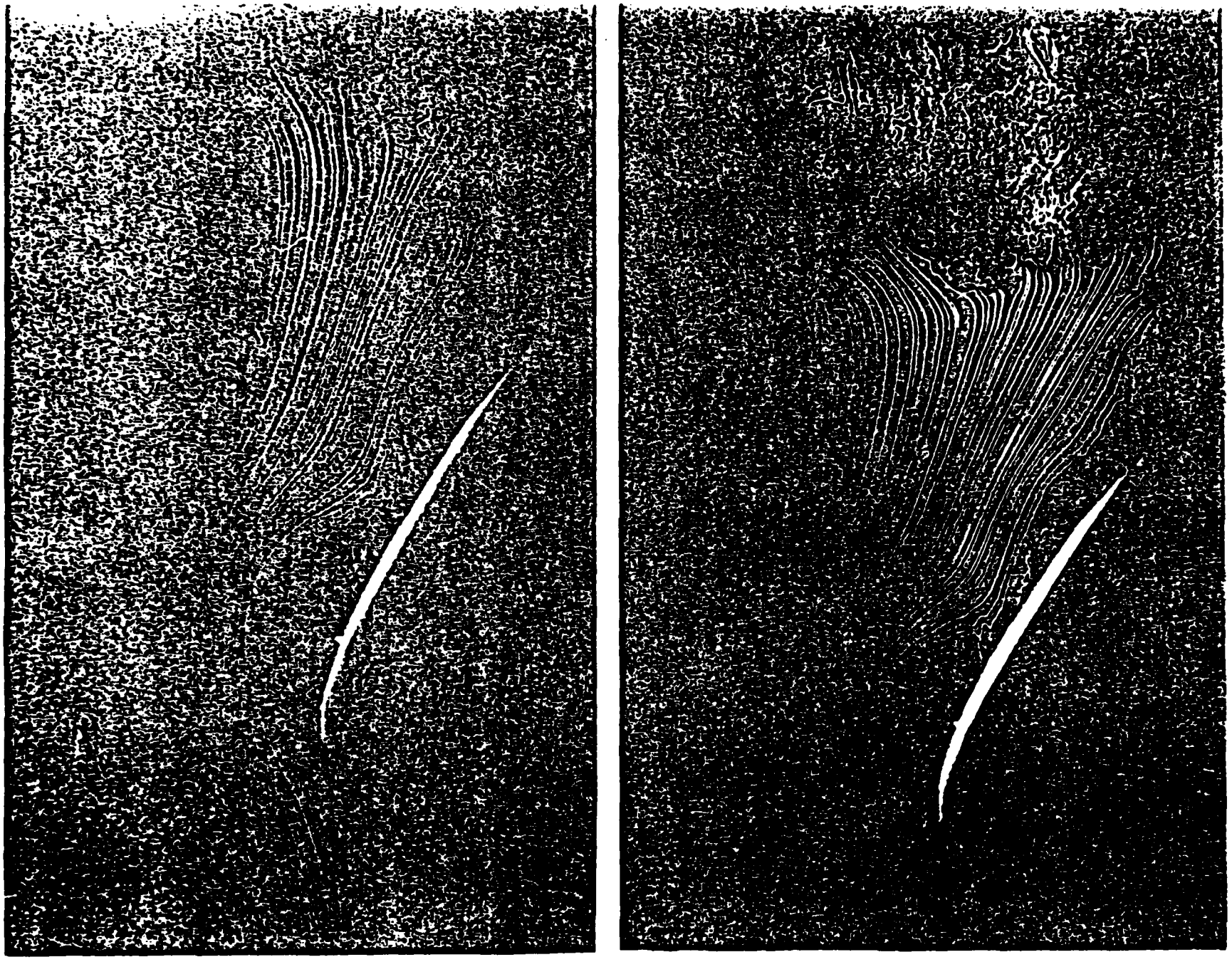

and was less well defined both inboard of the tip and out from the tip, in the mean flow. As seen in Fig. 23, the wing tip vorticity for a static airfoil moves across the wing spanwise as it simultaneously moves toward the airfoil trailing edge. At $\alpha = 10^{o}$ and Re number 60,000 the toroidal tip vorticity moves approximately 4 cm inboard before being shed into the wake. The periodicity of the toroidal flow at $\alpha = 10^{o}$ is approximately 4-5 chords per cycle. Larger angles of attack produce reduced periods for the tip vorticity. And, indeed, this increased or decreased, angle-dependent vorticity becomes a striking flow feature during wing oscillation. Regardless of the induced strength of the tip vorticity, the streamlines remain well-behaved and evidence of turbulence is negligible. This flow characteristic perseveres well beyond the static stall angle where flow located spanwise toward the root shows easily identifiable flow separation. Finally, as separated flow envelops more of the chord, the toroidal vorticity of the wing tip begins to reflect the turbulence by dispersed streamlines evidenced in the wake.

Leading Edge Vorticity

The motion of the wing when oscillated beyond the static stall angle resulted in the expected generation of a leading edge vortex. At appropriate test conditions, the elicited vorticity exhibited the general characteristics described above for our experiments with oscillating airfoils and flat plates. The vorticity was most similar to that of previous work when located (or visualized) at distances >10 cm. inboard from the tip of the wing.

The examples of leading edge vorticity shown in Fig. 24 were obtained at Re number = 50,000, $\alpha_m = 15^{o}$, $\alpha_\omega = \pm 10^{o}$ and K = 0.5. The span location was 15 cm inboard from the tip. We found it necessary to use $\alpha_\omega = \pm 10^{o}$ since $\alpha_\omega = \pm 5^{o}$ appeared to be ineffective in eliciting a well-defined leading

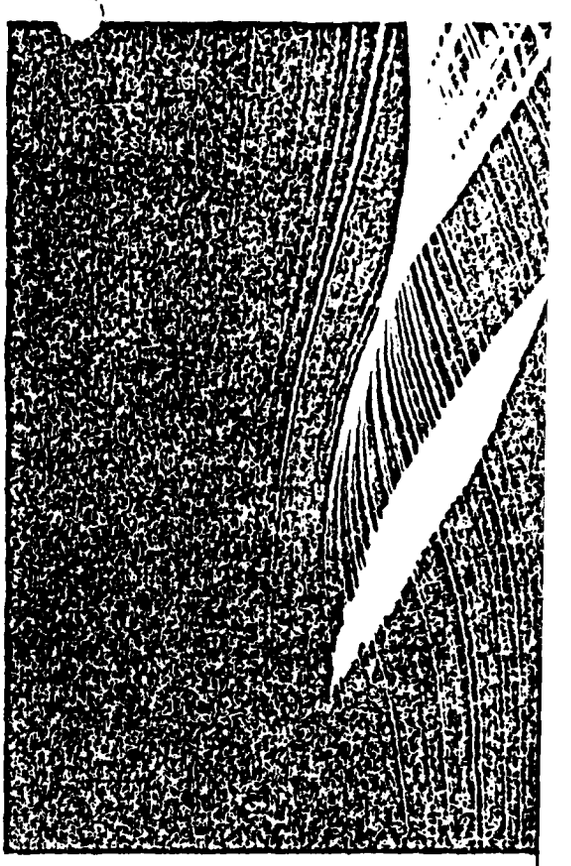

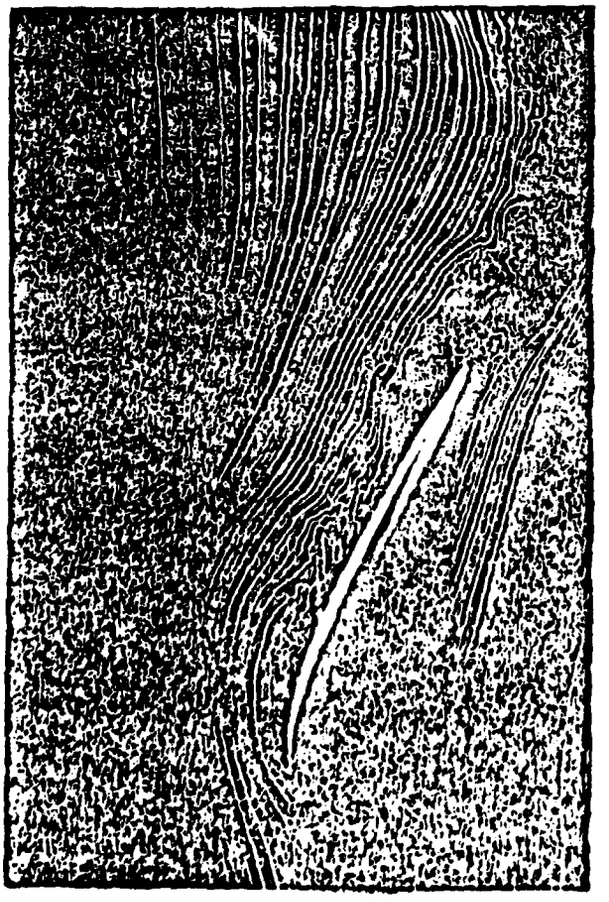

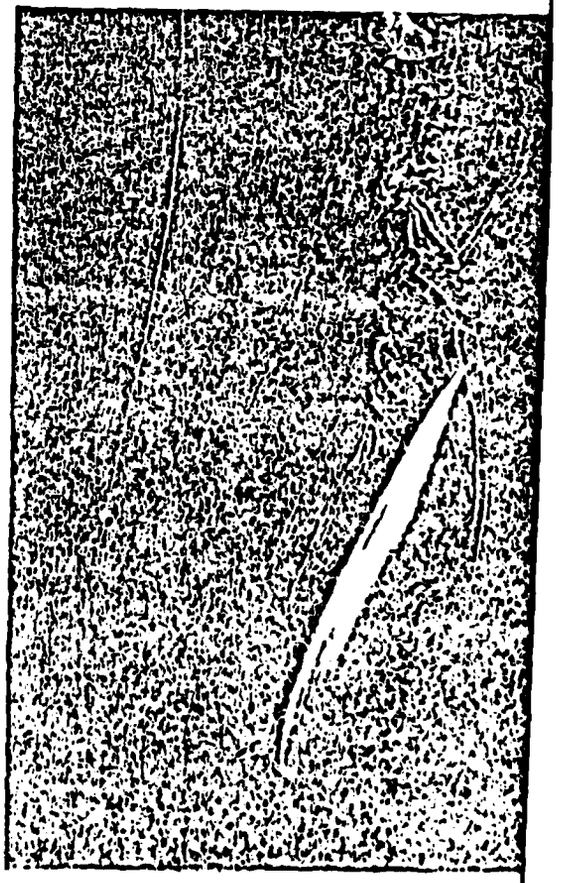

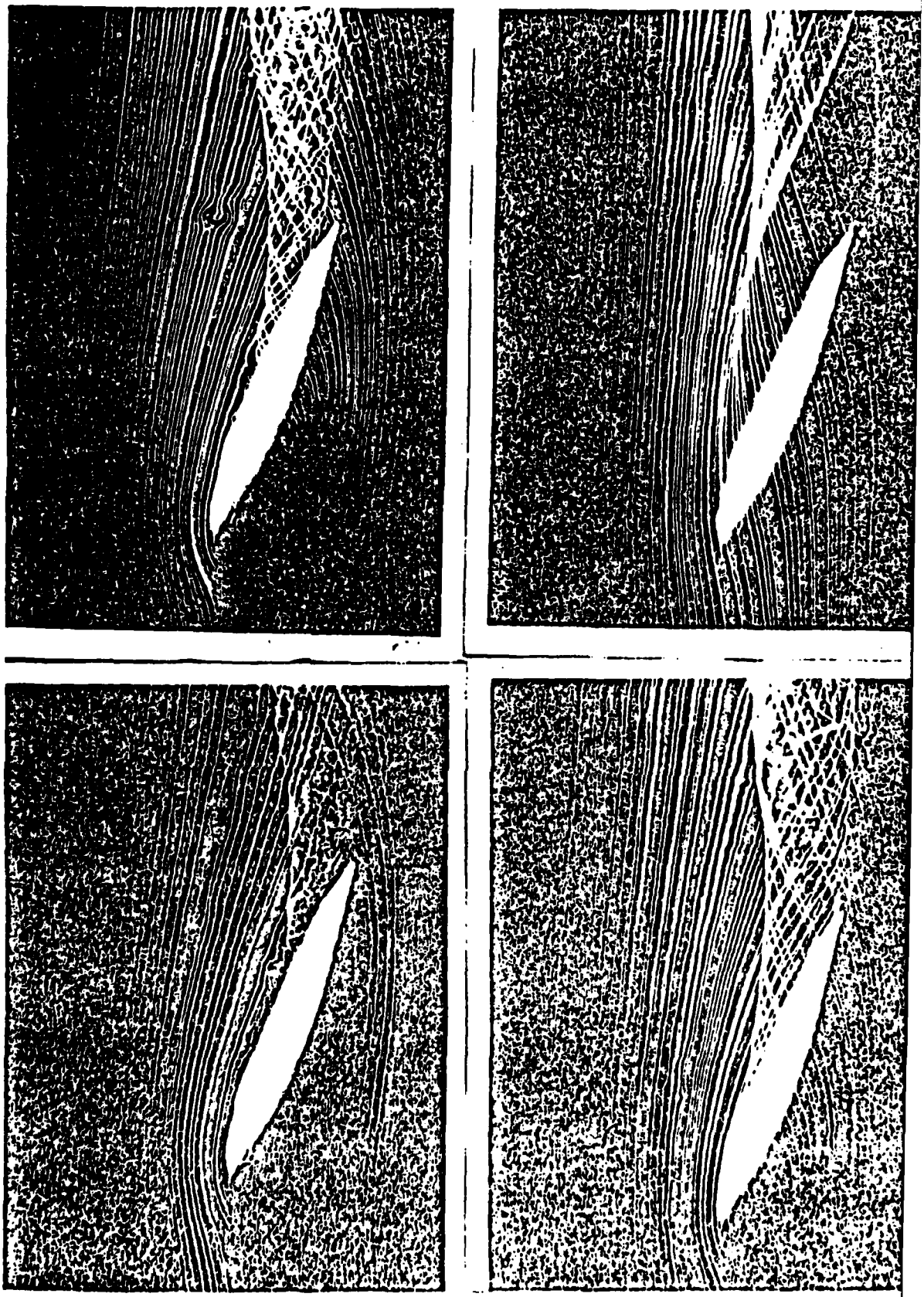

edge vortex. As noted above the vortex is both large and well-defined. In contrast to our observations on airfoils and plates, the vorticity was generated as the airfoil began decreasing the angle of attack from the maximum α of the oscillatory cycle. We expected the vortex to appear earlier in the oscillatory cycle. The second contrast, observed repeatedly, was the sawtooth appearance of outer streamlines and downstream vortical streamlines. The inherent cohesiveness of the vortical structure seen in our two-dimensional studies appeared to be yeilding to an additional influence in these three-dimensional tests. These differences will be discussed in the next section of this report.

Leading Edge and Tip Vorticity Interactions

In an attempt to probe the possible contributions of both leading edge vorticity and tip toroidal vorticity to the flow patterns about a wing, flow visualization was prepared in small spanwise steps. The test conditions (50,000 Re number, $\alpha_m = 15^o$, $\alpha_\omega = \pm 10^o$ and K - 0.5) assured the presence of a dominant leading edge vortex inboard and a dominant toroidal vortex at the tip of the wing. The visualizations of Figs. 25 and 26 summarize the resulting spanwise survey of flow disturbances.

As the flow is surveyed in two-dimensional sheets from the point of leading edge vortex dominance, it is clear that the leading edge vortex develops later in the oscillatory cycle as the tip of the wing is approached. Across the same spatial dimension, the leading edge vortex appears both smaller and weaker. At a spanwise point of about 5-7 cm from the tip, evidence of a leading edge vortex all but disappears.

Visualizing the flow at the tip of the wing and at 1 cm steps more inboard along the span results in observed distortions of the characteristic toroidal vorticity. The flow about the wing tip and into the tip wake

exhibits the usual [illegible]

altered angles of attack. At this spanwise position only for wake structures suggests the presence of other spanwise flow disturbances. When the flow is visualized for 1 cm inboard of the tip, these disturbances are more clear. The smooth toroidal bend of the streamlines from under to over the wing apparently encounter a much higher velocity field generated inboard. At certain points both spanwise and chordwise, the smooth streamlines are bent radically toward the upper surface of the wing. The normal inboard flow of these streamlines is, thus, truncated and does not wash across the normal amount (static conditions) of wing surface spanwise.

The interactions between tip vorticity and leading edge vorticity are difficult to show by flow visualization. The prominent features of both flow disturbances are apparently sacrificed to the interaction of the two. This is not simply a matter of complex cross products arising from two complex flows. Rather, the interactions appear to prevent the normal development of these prominent vortices. The conditions necessary to sustaining these structures are lost.

These studies are not completed. More detail will be forthcoming as different points of the oscillatory cycle are examined and as more experimental parameters are systematically altered. To date, the smoke wire work has been suitable. It has been corroborated by studies using titanium tetrachloride applied to the wing surface. In addition, files are being generated for the use of computer synthesized three-dimensional views of the ensuing flow. Many of these approaches are to be summarized by the student working on this project at an upcoming AIAA Student Paper Conference.

What we can conclude at this time is that pitching wings elicit a complex flow pattern in which three-dimension flows become critical. The

leading edge vortex, with the promise of lift enhancement, seems adversely affected by the proximity of a wing tip. Perhaps the lift enhancement potential of such vorticity will be completely lost to wing tip effects. We believe our observations do not support such a potentially complete loss. In addition, it appears that wing tip vorticity may decrease the cataclysmic stall associated with a trailing edge vortex and the leading edge vorticity may actually decrease wing tip vorticity drag. In other words, the three-dimensional problems of unsteady flows require considerably more attention.

Accelerating Flow

In addition to the work summarized to date (cf., Appendix), ongoing studies will first characterize the lift and drag experienced by an airfoil in accelerating flow. A force balance has been manufactured to fit the test section of the large, low-turbulence, 3'x3' wind tunnel to accommodate such testing. The results will provide a correlation between the intricate flow structures observed during accelerating the flow from rest and the forces actually experienced by the NACA 0015, 14" chord airfoil.

To associate these findings with existing literature (cf., Oshima et al., 1983) comparisons of the vortex-shedding frequencies for accelerating versus steady flows will be examined with the NACA 0015 airfoil exhibiting various angles of attack. The lift and drag characteristics may well reflect the shedding frequencies as a modified street frequency.

In order to match the results obtained in other portions of the project, the three-dimensionality of elicited flow structures also will be studied. The first step in these studies is to visualize accelerated flow structures from over the airfoil surface. In a similar matching effort, the acceleration flow structures will be examined for decay characteristics and the flow effects of acceleration followed immediately by deceleration will be examined.

Overall, these studies should provide the needed benchmark information for elaborating upon the unsteadiness elicited by an oscillating airfoil. Such information should move the work quickly and directly toward the understanding of exploitable lift enhancement mechanisms.

Theoretical Studies

Substantial progress has been made in the theoretical part of the research within the supported one-year period. Two papers have been published, one paper has been accepted for publication in a journal, two papers have been accepted for presentation in a professional conference, and two pieces of work are near completion. They are described separately in the following summary.

(1) "Trapping of a Free Vortex by Joukowski Airfoils," by M.-K. Huang and C.-Y Cho AIAA Journal, Vol. 20, No. 3, March 1982, pp. 292-298.

In this paper we have found that a free vortex can be captured by an airfoil for lift augmentation. The equilibrium position of the vortex at which it becomes stationary is determined by the vortex strength, airfoil shape, and angle of attac A linearized stability analysis shows that only some of the equilibrium positions near the trailing edge are stable. Increasing either camber or angle of attack decreases the vortex-trapping ability of the airfoil, whereas increasing thickness enhances it.

(2) "The Initial Lift and Drag of an Impulsively Started Airfoil of Finite Thickness," by C.-Y. Chow and M.-K. Huang, Journal of Fluid Mechanics, Vol. 118, May 1982, pp. 393-409.

An unsteady flow analysis is used to calculate the initial lift and drag of an airfoil that starts impulsively from rest. For a Joukowski airfoil with a cusped trailing edge, it is found that increasing either camber or angle of attack will cause increases in both initial lift and drag, whereas increasing thickness will result in an opposite effect. Effects of trailing-edge angle are examined by considering the symmetric Karman-Trefftz airfoil. The result shows that both lift and drag vanish at the initial instant if the airfoil has a finite trailing-edge angle. The analytical solution obtained in this paper will help us later in the numerical computation of various unsteady flows about an airfoil.

(3) Apparent Mass Coefficients for Isosceles [illegible]
by Two Circles," by M.-K. Huang and C.-Y Chow, a paper accepted for publication by Journal of Aircraft.

Closed-form solutions are obtained for the apparent mass coefficients of an aircraft fuselage whose cross-section has the shape of either an isosceles triang or a configuration formed by two circular arcs. These coefficients are needed in computing aerodynamic forces acting on the fuselage of varying cross-sectional area. Based on the exact solutions, we find that the area-equivalence rule, an approximating method that is often used in preliminary designs, can hardly be use to estimate the forces on all of the fuselages considered in this paper.

(4) "The Unsteady Boundary Layer on an Elliptic Cylinder Following the Impulsive Onset Translational and Rotational Motion," by D. F. Billings and C.-Y. Chow, a paper to be presented in AIAA 21st Aerospace Sciences Meeting in January 1983.

The unsteady fluid motion about an elliptic cylinder impulsively set into translational and rotational motion is obtained by the method of matched asymptotic expansions for small time and large Reynolds number. It is found that a pitch-up motion is capable of preventing the early formation of a leading edge separation bubble on a cylinder traveling at an angle of attack. In the presence of a rotation, the onset of an adverse pressure gradient is displaced rearward from its location for pure translation. Influences of rotation on vorticity distribution and flow structure are examined in detail.

(5) "Unsteady Flows About a Joukowski Airfoil in the Presence of Moving Vortices by C.-Y. Chow and M.-K. Huang, a paper to be presented in AIAA 21st Aerospace Sciences Meeting in January 1983.

The motion of discrete vortices in the vicinity of a Joukowski airfoil and the influence of these vortices on airfoil lift and drag are computed using a co puter code that has been written based on conformal mapping and unsteady flow

analyses. Studies are made on the stability of a trapped vortex when perturbed away from its equilibrium position with a finite displacement, on the release of a free vortex at a location upstream from an airfoil, and on the behavior of a moving vortex of increasing strength. Numerical results indicate that under various arrangements moving vortices can be utilized to generate high lift or thrust on an airfoil.

(6) Numerical Study of the Unsteady Flow Caused by Vortices Released Intermittently from the Upper Surface of an Airfoil.

This work is still under investigation. The vortex train used in the mathematical model is adapted to simulate the flow generated in the wake of an oscillating spoiler moving into and out of the airfoil surface. Computations have been made for various vortex strengths and oscillational frequencies. It has been found that the time-averaged lift is increased by continuous release of vortices. We are looking for the optimum frequency that would maximize the lift. The result will be submitted to a journal for publication.

(7) Effect of Suction or Blowing Normal to the Airfoil Surface on the Trapping of a Free Vortex.

This is a theoretical study inspired by the experimental work being performed in the Army Aeromechanics Laboratory at Ames Research Center. It has been observed in that experiment that a vortex formed by leading-edge separation can be trapped stably on an oscillating airfoil by applying suction or blowing at the midchord station on the upper surface. In the first step of our analysis the airfoil is not oscillating, and suction or blowing is achieved by putting a source or sink on the airfoil surface. Results show that suction indeed stabilizes the vortex trapped near the trailing edge. We are summarizing our findings and will submit the work for journal publication. In the next step of our study on this phenomenon the analysis will be extended to the case of an oscillating airfoil.


FILM
4-8